Next Generation Anodes for Lithium-Ion Batteries

Third Quarter Progress Report 2020

Jack Vaughey
Argonne National Laboratory
9700 South Cass Avenue
Lemont, IL 60439
Phone: (630) 252-8885
E-mail: vaughey@anl.gov

Brian Cunningham, DOE-EERE-VTO Program Manager
Hybrid Electric Systems, Battery R&D
Phone: (202) 586-8055
E-mail: brian.cunningham@ee.doe.gov

Table of Contents

Silicon Deep Dive Overview

Project Introduction

Silicon has received significant attention as an alternative to the graphitic carbon electrode presently used in lithium-ion batteries due to its high capacity, stability, and availability. Compared to graphitic carbon, elemental silicon's capacity is nearly an order of magnitude higher (~3600 mAh/g silicon vs 372 mAh/g Graphite), however, problems including large crystallographic expansion (~320%) upon full lithiation, slow lithium diffusion, and high reactivity at high states of charge have hindered full scale commercialization. In a cell, these electrochemical and diffusion issues are manifested as particle cracking, particle isolation (binder failure), electrolyte reactivity, and electrode delamination issues. Because of the technological advances possible if a silicon anode can be designed and proven, researchers in multiple disciplines have pushed to understand these physical issues and advance the field and create a viable silicon-based electrode.

Next Generation Anodes for Lithium-Ion Batteries, also referred to as the Silicon Deep Dive Program, is a consortium of five National Laboratories assembled to tackle the barriers associated with development of an advanced lithium-ion electrode based upon silicon as the active material. This research program has several goals including (1) evaluating promising silicon materials that can be either developed internally, in association with private companies, or from academic collaborators in quantities sufficient for electrode preparation by the consortiums facilities, (2) developing a silicon-based electrode that meets BatPaC specifications, and (3) executing full cell development strategies that leverage DOE-EERE-VTO investments in electrode materials and characterization. The primary objective of this program is to understand and eliminate the barriers to implementation of a silicon-based anode in a lithium-ion cell. The five National Laboratories (ANL, NREL, LBNL, ORNL, and PNNL) involved are focused on a single program with continuous interaction, clear protocols for analysis, and targets for developing both an understanding and a cell chemistry associated with advancing silicon-based electrodes for lithium-ion cells. This undertaking is a full electrode/full cell chemistry project with efforts directed at understanding and developing the chemistry needed for advancing silicon-based anodes operating in full cells. Materials development efforts include active material development and evaluation, binder synthesis, surface functionalization, safety, strategies to mitigate lithium loss, and electrolyte additives. Efforts include cross-lab diagnostic research including a wide range of electrochemical, chemical and structural characterization of the system across length- and time-scales. Specialized characterization techniques developed with DOE-EERE-VTO funding, include neutrons, MAS-NMR, optical, and X-ray techniques being employed to understand operation and failure mechanisms in these silicon-based anodes. The project is managed as a single team effort spanning the Labs, with consensus decisions driving research directions and toward development of a functioning stable silicon-based electrode.

The Silicon Deep Dive project seeks to identify the limiting factors of silicon-based electrodes that need to be overcome to produce a viable functioning LIB electrode and full cell. The issues include understanding and controlling silicon surface chemistry, lithium loss due to side reactions, active material interactions, and the role of electrolyte stability. The goal of the project is to utilize our understanding of silicon and silicide reactivity, electrode formulation, and binder and electrolyte formulations, to design a functioning silicon-based electrode for a lithium-ion cell that meets DOE-EERE goals. Combined with the SEISta's efforts focused on interfacial reactivity, key variables can be isolated and studied to improve the performance of a silicon-based cell. This interaction is maintained and accomplished through joint meetings, face to face discussions, and extensive collaborations between the teams.

FY20 Deep Dive Goals:

FY20Q1	Evaluate two new binder - slurry – silicon laminate combinations that lead to improved stability and a 15% improvement in performance compared to baseline for a high silicon-loading (>60%) electrode.
FY20Q2	Assess and evaluate multiple surface driven coatings that utilize a multivalent surface substitution. Develop an understanding of the formation mechanism on the cycling stability of the underlying silicon electrode; propose a mechanism of formation.
FY20Q3	*Assess the stability of electrode level silicon baseline materials on cycling and determine the range of species that solubilize and leach into the electrolyte.*
FY20Q4	Combine the advancements made over various aspects of the silicon electrode by the Silicon Deep Dive team evaluate them at the full system level and optimize a best full cell with a commercial cathode that using BatPaC can be determined to deliver > 350 Wh/kg for 120 cycles; Evaluate the energy fade on standing for 2 mos and demonstrate an improvement over baseline of 20%.
FY20Q4	*Have published a document that will enable other research and development groups to analyze stability of the SEI on a silicon-based anode, thus enabling developers or researchers to continually improve silicon cell stability (joint milestone with the SEISta).*

Approach

Oak Ridge National Laboratory (ORNL), National Renewable Energy Laboratory (NREL), Pacific Northwest National Laboratory (PNNL), Lawrence Berkeley National Laboratory (LBNL), and Argonne National Laboratory (ANL) have teamed together to form an integrated program. Technical targets have been developed and regular communications have been established. Throughout the program, there is a planned focus on understanding, insights into, and advancement of, silicon-based materials, electrodes, and cells. All anode advancements will be verified based on life and performance of full cells. Toward that end, baseline silicon-based materials, electrodes, and cells have been adopted, along with full cell testing protocols.

In examining improvements, changes to the baseline cell technology will be minimized. As an example, silicon active material coating improvements will be verified on baseline silicon materials in electrodes fabricated by the battery research facilities. All other components in the prototype cells (i.e. positive electrode, separator, and electrolyte) will be from the baseline technology. While there are many testing protocols that can be utilized to benchmark the baseline technology, this program has adopted a testing protocol from the literature that has worked well for lithium-ion cells with silicon containing anodes. Shown pictorially in **Figure 1** the test starts with three slow (C/20) formation cycles, an HPPC cycle, and then the C/3 aging cycles. The test ends with another HPPC cycle and three more slow (C/20) cycles. All constant current cycling is symmetric between charge and discharge rates. The tests are run at 30°C. If there is little or no aging in the first 100 cycles, the protocol can be repeated. This protocol effectively examines capacity, impedance, and aging effects in about a month's worth of testing. As the program matures, materials developments will be incorporated into baseline silicon-based materials, electrodes, and cells. Scale-up of materials, incorporation of materials advancements into electrodes and prototype cells, and characterization and testing of cells, as well as evaluation of safety and abuse tolerance are part of a wide range of integrated studies supported by battery research facilities at the National Labs working closely with the program. These research facilities include the Battery Abuse Testing Laboratory (BATLab), the Cell Analysis, Modeling, and Prototyping (CAMP) facility, the Materials Engineering Research Facility (MERF), and the Post-Test Facility (PTF). At the present time the baseline silicon is from Paraclete Energy (Chelsea, MI).

The fundamental understanding of silicon-based electrode active materials is based on extensive electrochemical and analytical diagnostic studies on components, electrodes, and cells conducted within the program. This effort contains in-situ and ex-situ studies on full and specialty cells, including reference electrode

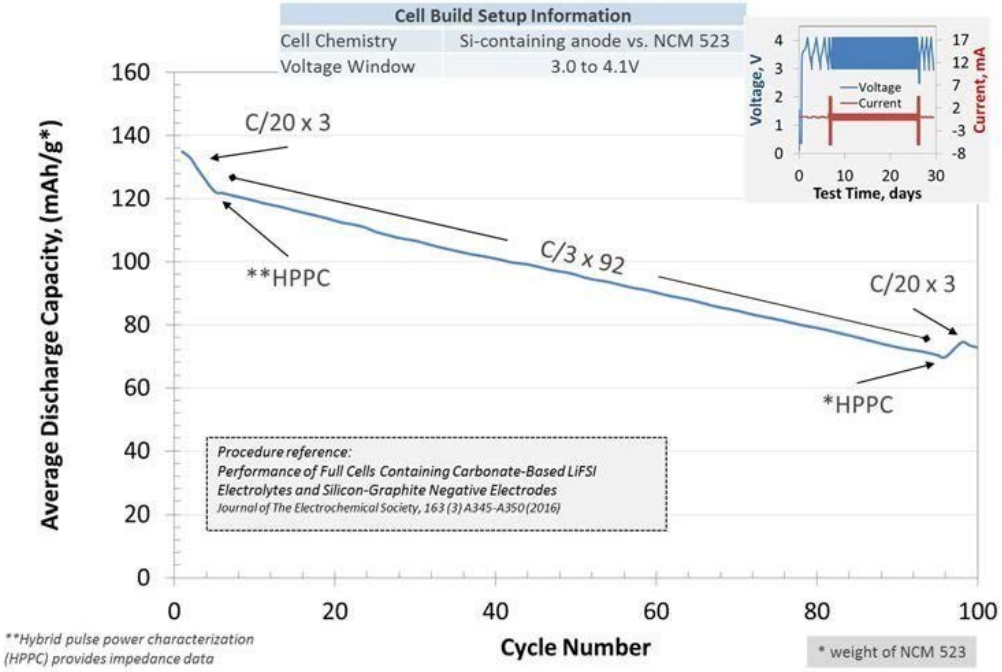

Figure 1. Full cell testing protocol.

cells. Overall, the diagnostic studies are intended to help establish structure-composition-property relationships, including lithium-reactivity at the silicon surface and bulk transport and kinetic phenomena. Additionally, these studies form the basis for accurately assessing component and electrode failure modes.

Supported by diagnostic studies, materials development on silicon-based materials, electrodes, and cells is being conducted to enhance interfacial stability, accommodate volume changes, and improve overall performance and life. Key to this effort is the development and testing of coatings and additives designed to modify and stabilize the dynamic silicon-electrolyte interface. Further, functional polymer binders designed to accommodate volume changes, increase conductivity, and improve adherence are being developed and analyzed. Finally, the program is exploring active material development, including hydride or organically functionalized silicon, silicide materials, high surface area passivated silicon created by high energy ball-milling, and thin films.

Communication of programmatic progress to the battery community is critical. This will generally be accomplished through publications, conference and AMR presentations, reports, and reviews. Further, the program is open to industrial collaboration that does not limit program innovation or the free flow of information. Finally, this program is highly integrated with our sister program on SEI-Stabilization (SEISta), centered at NREL. In general, SEISta is focused on the development and characterization of model systems, well-defined active area thin film electrodes, silicon wafers, and interfacial phenomena (e.g. SEI formation, changes, and growth).

Milestone Update FY2020Q3

(1) Assess the stability of electrode level silicon baseline materials on cycling and determine the range of species that solubilize and leach into the electrolyte.

(2) Publish a document that will enable other research and development groups to analyze stability of the SEI on a silicon-based anode, thus enabling developers or researchers to continually improve silicon cell stability (joint milestone with the SEISta).

The main Q3 milestone asks to assess the stability of electrode level silicon baseline materials on cycling and determine the range of species that solubilize and leach into the electrolyte. For this effort we tasked two DeepDive groups (C. Johnson, G. Liu) to take the lead and develop the analytical tools necessary to determine the types of species that are found in the electrolyte as solubilized SEI products. For the solid silicon SEI components identified in the literature, research efforts have identified several polymerized ring-opened solvents (FEC, EC), various salts including inorganic (Li_2CO_3) and coordination salts (i.e. LiEDC). Notably the latter, identified by the Ross Group at LBNL, has been seen to be a significant component that appears to have spectroscopic handles that allow its identification in the solid SEI films (Han Group, Key Group, Kostecki Group). LiEDC was later synthesized by Lu Zhang and found to form readily and, once purified, be relatively insoluble in the solvents commonly used on out electrolytes. The insoluble nature of the materials makes identification and isolation more straightforward. However, in the silicon systems under study, it has been noted that the SEI layers on the anode are not dimensionally stable. On cycling the height, thickness, and weight of the SEI have been observed to change as a function of state of charge (SOC). Using Rotating Ring Disk Electrochemistry (RRDE), Johnson et al., noted in previous reports that the SEI appears to show the most dramatic changes in volume above 450 mV (vs Li), while Sa, et al., has seen dramatic weight and density shifts using EQCM-D. As the weight is changing as a function of state of charge, the conclusion drawn is that species in the SEI are oxidizing near those voltages and becoming soluble. Identification of these species is important as soluble species in the electrolyte may re-reduce on charge, and precipitate on the anode, transfer to the cathode and further react, or possible change the transfer kinetics of the lithium cations in the electrolyte. Quarterly reports last year by Key and Vaughey utilized Li_7Si_3, an intermediate compound formed in the charged state of silicon anodes near 300 mV, to note that even at this SOC significant degradation of ring-electrolytes was observed by MAS-NMR. In this case EC (or FEC) was seen to degrade as it accepted electrons from the reduced silicide on contact. Although made in a controlled environment, the exact nature of the reduced species was not identified, although the C-F bond in the FEC was maintained. A similar observation was seen with PVDF binders, where C-F bonds were stable and degradation reactions occurred at polymerization defects (-CH2-CH2-) rather than at random spots.

In this quarter, C. Johnson had been developing his RRDE methods and been applying them to solubilized species coming off as degradation products using a Si thin film cell (provided by G. Veith ORNL). Earlier reports (FY19Q3-FY20Q2) highlighted technique development efforts using redox mediators to track SEI conductivity vs SOC, the role of surface charge carrier, and FEC electrolyte additives. Work with FEC noted that measurable redox active species are coming off of 70% Si drop-cast electrode at SEI formation and during simultaneous sweep at the Pt ring electrode, in addition the FEC (via its film formed) was playing a role of surface passivation to these species, suggesting classic pre-passivation of the Si SEI. Further effort will continue once the COVID19 situation is resolved and safe lab practices can be re-established.

Over the past few months, Gao Liu at LBNL has been focused on the development of techniques to isolate and identify soluble SEI species. His work has two focus areas – a post-cycling gradient wash technique that uses polarity to solubilize and separate species formed but trapped in the SEI and FTIR, a spectroscopic technique useful for identification of organic species. The gradient solvent wash was developed with his group to isolate

and identify species that formed but due to isolation techniques were often mixed together. Using mixtures of ethyl acetate and hexane, he was able to create a gradient of polarity that selectively dissolved out species

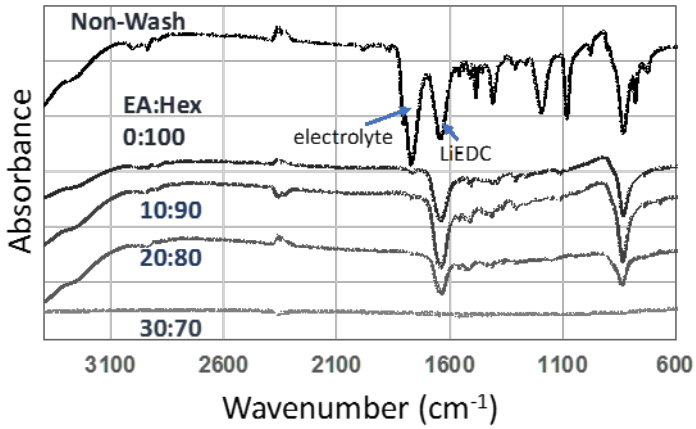

Figure 1. FTIR spectra of species remaining on a Cu electrode after gradient wash with hexane-rich mixtures. LiEDC, a common salt seen on the surface, was found to be soluble in solvent mixtures with greater than 30% ethyl acetate.

in the SEI by their relative iconicity, salts, to alcohols, to simple oligiomeric species. Earlier work (FY19Q2-FY20Q2) reported on its utility for test cells (Cu with Gen2, VC), however due to the COVID19 situation, further work has been on hold until the pandemic is resolved and safe lab practices can be re-established. Further work will include using FEC species and assessing the differences in SEI between species generated in Gen2, Gen2/FEC, and Gen2/FEC/Zintl additives (with Key, Dogan, & Sa).

Additional work to identify the solubilized species within the DeepDive silicon has been done in conjunction with the Post-Test facility (PT). Zhen Zhen Yang has initiated additional EQCM-D work in association with Prof Sa (UMass) to evaluate the role of SOC on SEI thickness and composition. Utilizing the spectroscopic tools available, including XPS (insoluble surface films), Raman Spectroscopy (insoluble surface films), and electron microscopy (surface degradation), combined with GC-MS, various species can be identified and certain species can be eliminated as possibilities (notable in the various ring opening pathways associated with FEC).

Overall, the FY20Q3 milestone is incomplete. Although the work building up to the report was initiated last year and technique development initiated in our baseline systems, the halt in work due to the COVID19 outbreak has limited progress of the efforts since March 2020. As researchers are gradually getting back to work at the DeepDive institutions, the work towards the Q3 milestone will resume and be reported as part of the FY20Q4 report later in the year.

In preparation for the FY20Q4 milestone, a combined DeepDive and SEISTA effort has been undertaken at constituent labs (SNL, ORNL, NREL, ANL) to continue testing, evaluation, and protocol formulation in support of publishing a document that enables other research and development groups to analyze stability of the SEI on a silicon-based anode, thus enabling developers or researchers to continually improve silicon cell stability. In FY20Q3, the work and cells required to develop and create the protocols needed by the FY20Q4 milestone were prioritized by the teams. Significant progress towards development of a silicon testing protocol (based on using an $LiFePO_4$ cathode) has been established and used by internal teams to create a preliminary calendar prediction model for silicon LIB anodes. More detail can be seen in their preliminary report starting on page 11. Team members included Chris Johnson, Max Schulze, Marco Rodrigues, Josey McBrayer, Chris Apblett, Ira Bloom, Andrew Colclasure, Gabriel Veith, Xiaolin Li, and Nathan Neale.

Silicon Electrode Studies

Calendar-Aging of Full Cells with High-Content Silicon Negative Electrodes

Mei Luo, M.-T.F. Rodrigues, D.P. Abraham

Background

The use of blended silicon-graphite (Si-Gr) negative electrodes increases the energy density of lithium-ion cells over those containing only graphite (Gr) electrodes. However, volume changes in the active Si particles that occur during cycling causes deterioration of the solid-electrolyte interphase (SEI) layer on the particles resulting in further electrolyte reduction. This consistent background reaction can immobilize Li^+ ions and lead to capacity fade. Another concern is the calendar-aging of Si-based electrodes – here, performance degrades even though the cell is not being cycled. Determining the mechanisms of, and establishing protocols for, calendar-aging has become a high-priority task in our silicon programs.

Various approaches are being pursued to improve the performance of silicon-based LIB anodes, including

- optimally sized Si to prevent particle fracture and minimize surface area-based reactions with the electrolyte,
- binders that help create a conductive framework while maintaining electrode integrity during cycling,
- electrolyte additives that enhance the stability of the silicon particle-electrolyte interface, which is continually disrupted during silicon expansion and contraction exposing fresh surfaces for solid electrolyte interphase (SEI) formation that trap additional lithium.

Since silicon and graphite respond differently to the binder, electrolyte additives, etc., high silicon (no graphite) electrodes were used to yield insights into the reactivity of the silicon in the cell. Here we present the calendar-aging performance of full cells prepared using "4KD" silicon particles from Paraclete Energy; these Si particles have a native oxide layer and no additional coatings. The composition and constitution of the electrodes used in the full cells are as follows:

- 80% 4KD Silicon, 10% carbon black, 10% LiPAA binder (CAMP A017) – Negative Electrode
- 90% NMC532 ($LiNi_{0.5}Mn_{0.3}Co_{0.2}O_2$), 5% carbon black, 5% PVdF (CAMP C013B) – Positive Electrode

Measurements were conducted in cells equipped with a reference electrode (RE). Each cell contained 20.3 cm^2 electrode disks spaced by two layers of a 25 µm thick microporous separator (Celgard 2325) and Gen2 + 10 wt% FEC electrolyte. Lithium metal was plated *in situ* onto the tip of a thin copper wire (25 µm dia.) to form a microprobe RE; this lithium RE was sandwiched between the separators and provided information on the positive and negative electrode potentials. The cells were tested as described below.

Results

Cell voltage and electrode potential profiles during cycling are shown in **Figure 1**. The test protocol consists of the following: 3 (formation) cycles between 3-4.1V followed by an initial HPPC (pulse-current) test to measure impedance; charge to 4.1 V and calendar-aging hold for 300 h; final HPPC test, followed by 3 final (diagnostic) cycles between 3-4.1 V. All cycling is conducted using the same current. **Figure 1** indicates the following:

- Time required to complete the final 3 cycles is smaller than the time required to complete the first 3 cycles. Because the cycling current is the same, this observation indicates that the cell has lost capacity during the test.

- During the 330 h hold, the cell voltage is maintained constant. However, the negative and positive electrode potentials increase by about 60 mV. The negative electrode potential increase, from ~0.14 to ~0.20 mV, indicates loss of Li^+ ions from the silicon, most likely to the solid electrolyte interphase (SEI). Because the cell voltage is held constant, the positive electrode potential increases, from ~4.24 V to ~4.30 V, to match the negative; the positive potential change indicates increasing delithiation of the oxide particles. Note that these changes are seen even though there are no volume changes in the silicon particles.

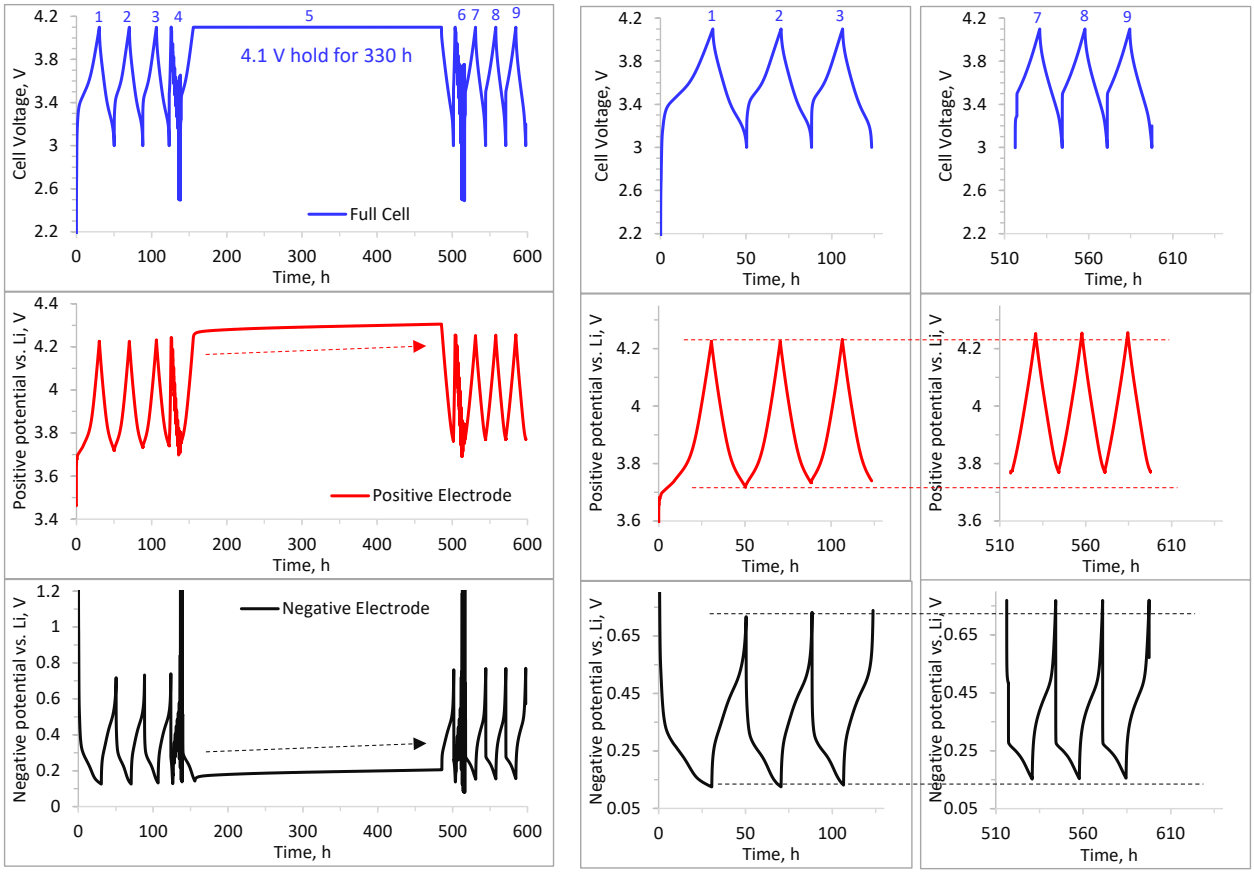

Figure 1 (Left Panel). Changes in the cell voltage, and positive/negative electrode potentials of a NMC532/80Si cell. Cycles 1-3 (formation) and cycles 7-9 (diagnostic) are at a ~C/20 rate, cycles 4 and 6 are HPPC tests and cycle 5 includes the calendar-aging hold at a cell voltage of 4.1 V for 300 h. Right Panels show details of cycles 1-3 and cycles 7-9.

- The current flow vs. time during the 330 h calendar-hold is shown in **Figure 2**. The left panel shows the data on a linear scale, whereas the right panel shows the same data on a log-log plot. The fit equation indicates that the current shows an exponential decay early on and a power law decay at longer times. The power law exponent is ~0.5, which suggests that the long-term behavior is mainly governed by SEI growth on the negative electrode. Note that the current never drops to zero, indicating continuing charge transfer during the voltage hold even at 330 h.

- **Figure 3** shows results from the HPPC tests, which were conducted immediately before and after the calendar-hold. Note that the ASI data are plotted versus the electrode potential (and not the cell voltage): such plots take into account the electrode potential shifts that occur because of Li-inventory changes during the calendar-hold and the charge-cycle thereafter. For both electrodes the ASI at any given potential increases on aging. Note that the data shown are for discharge pulses, during which the oxide is lithiated and

the Si is being delithiated. That is, the ASI reflects the difficulty of lithiating the oxide and delithiating the Si. For the positive electrode, the impedance rise is higher at lower oxide potentials, whereas for the silicon electrode, the impedance changes are mainly seen at potentials > 0.5 V vs. Li. Studies are underway to examine the mechanisms and processes that cause these changes.

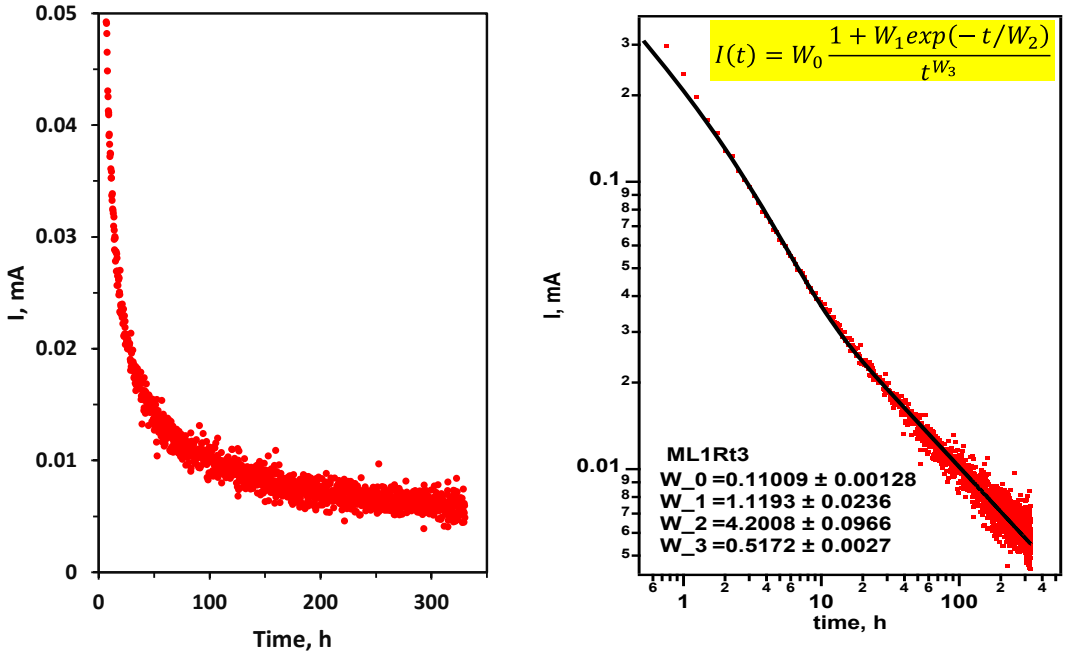

Figure 2 (Left Panel). Current change during the 330 h at 4.1 V. (Right Panel). Same data, plotted on a log-log scale. The inset shows the fit equation. The fit line is shown by the solid black line, whereas the red markers indicate the data points.

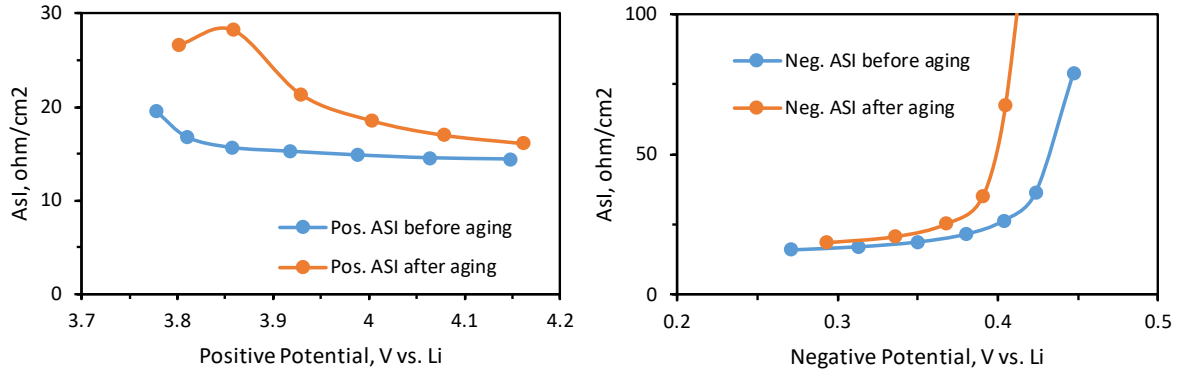

Figure 3. Area specific impedance (ASI) vs. electrode potential for the positive electrode (left panel) and negative electrode (right panel). Note that both the X- and Y-axes scales are different for each electrode.

- **Figure 4** shows the cycle 2 and cycle 9 potential-capacity profiles, both obtained at C/20 rate, as hysteresis plots. Note that the plots are per gram of oxide (or Si) in the positive (or negative) electrode at the beginning of the test. The differences between the cycles result both from the calendar-hold and from the cycles that follow it. Observe the oxide plots (left panel): (i) cycle 2 has regions with a shallow slope and a steeper slope, whereas cycle 9 only displays the steeper slope; (ii) discharge (oxide-lithiation) capacities at cycle 2 and 9 are 105.8 and 78.1, respectively, a difference of 27.7 mAh/g-oxide; (iii) the aged electrode cycles at higher potentials and shows a small hysteresis that is not apparent in cycle 2. For the Si electrode (right panel), the following observations can be made: (i) charge delivered (or removed) from the electrode is

lower during cycle 9 than cycle 2, indicating that less silicon is being cycled as aging progresses; (ii) the profile shape differences suggest changes in silicon lithiation behavior.

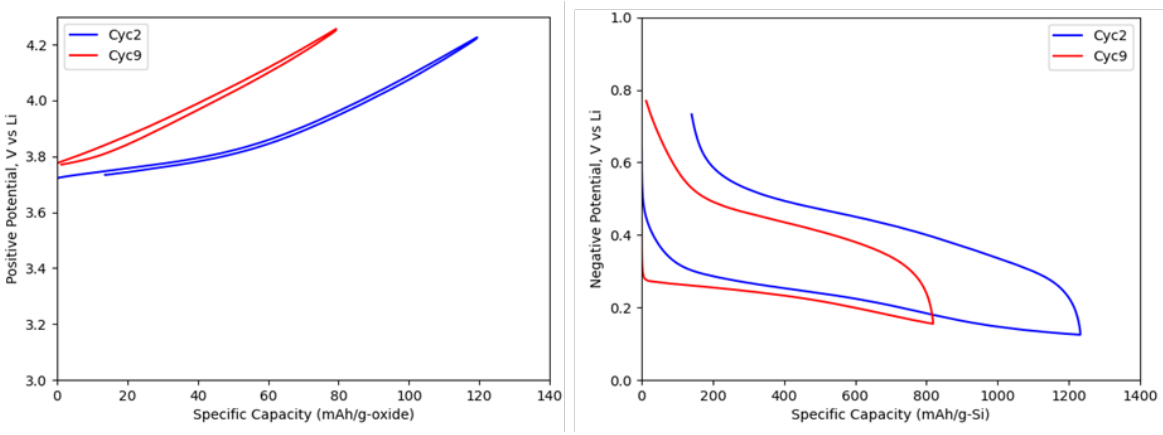

Figure 4. Potential-capacity profiles from cycle 2 (blue) and cycle 9 (red) of a NMC532/Si cell. Note that the capacity data are shown per gram of active material in the electrode (per gram oxide for the positive and per gram Si for the negative electrode).

Conclusions

We collected cycling data from an NMC532/80Si cell containing the Gen2 + 10 wt% FEC electrolyte. The highlights from our data are as follows:

- The positive and negative electrode potentials show a small increase during the 330 h calendar-aging hold at 4.1 cell voltage.
- During the voltage hold, the current shows an exponential decay initially and a power law decay at longer times. The current never drops to zero, indicating continuing charge transfer apparently to the negative electrode SEI, i.e., the SEI formed by the FEC is not sufficiently passivating and continues to dissolve and reform even though the silicon particle (and electrode) volume does not change.
- Cell impedance increases during the calendar-hold: this increase is observed for both electrodes. The impedance data apparently reflect changes in the Si particles that are induced by the lithiation-delithiation bond breaking and reformation processes.
- Additional diagnostic studies are underway to determine the mechanisms and processes occurring during the calendar-aging.

Cycle and Calendar-Lifetime Protocols for Silicon Based Anodes

Chris Johnson, Max Schulze, Marco Rodrigues, Josey McBrayer, Ira Bloom, Andrew Colclasure, Gabriel Veith, Xiaolin Li, Nathan Neale

Background

In this quarter we made significant progress working towards our joint Q4 milestone with the SEISTA program: Have published a document that will enable other research and development groups to analyze stability of the SEI on a silicon-based anode, thus enabling developers or researchers to continually improve silicon cell stability (joint milestone with the Silicon Deep Dive). The goal of this joint milestone was to utilize the knowledge base built from these silicon based programs to devise and disperse a standard testing cycle and calendar-lifetime protocols for silicon-based anodes. The protocols under development are designed to identify and provide insights into phenomena seen in early cell testing that can be correlated with poor cycle or calendar life. These may include active material loss, lithium inventory loss, and electrolyte degradation.

Justification: Silicon (Si) anodes are poised for implementation into advanced high-energy Li-ion batteries technologies. However, while Si cycle life is sufficient (>1000 cycles), the calendar life is sub-standard, typically seen to be less than 24 months life before unacceptable energy loss is realized. The calendar-life tests developed focus on a voltage hold in an LFP vs. Si anode full cell at high state of charge (3.35 V) (full lithiation @ equivalent ~ 100 mV vs. Li on the Si side, and delithiation @ equivalent ~3.45 V for LFP vs. Li on the cathode side). *Total test time is 290 h or about 1.5 weeks.*

The current (i) measured during the voltage hold is associated with an electrochemical reaction that is occurring in the system. It should follow that this electrochemical reaction represents (1) a rate of Li consumption (irreversible) and Li reaction (reversible) in the cell, and (2) any side reactions that occur at the electrodes (additives/solvent reduction, etc.). It is assumed that the LFP is essentially an inert electrode in this case only providing counter charge (or Li) to the extent needed. Thus, the charge consumption is only relevant to the Si electrode in the full cell with LFP. The current data collected is fit to a model to capture a projected calendar life. Tests involve two scenarios: (1) there is enough Li to supply an adequate Li inventory in the cell (oversized capacity LFP electrode), QLFP>>QSi and (2) the cell is 'balanced' with an n/p QSi/QLFP ratio of 1.05 – 1.1. This first condition will evaluate the best case scenario for the chemical and electrochemical qualifications of the Si material design (best current measurement breakdown). The second condition evaluates not only the loss of capacity (for whatever reason; Li irreversible) from the Si side during hold, but the difference in i measured between the two test conditions will indicate the stability or calendar life of the system.

Results

The calendar life problem is associated with an unstable passivating layer on the Si surface, even without the active cycling of lithium cations. In this effort we are developing an electrochemical testing protocol that is targeted towards gaining information about the calendar life of Si anodes. For quick turnaround, the test must be acquired over approximately a two week period, and then the data projected out to 5 years in order to make a life prediction, requiring a numerical model that is based on a low error fit.

The protocol proposed and under development uses a constant voltage hold and monitors the current (***Figure 1***). The accumulated capacity during the hold is summed and the capacity loss is checked on the second C/10 cycles compared to the initial C/10 formation cycles.

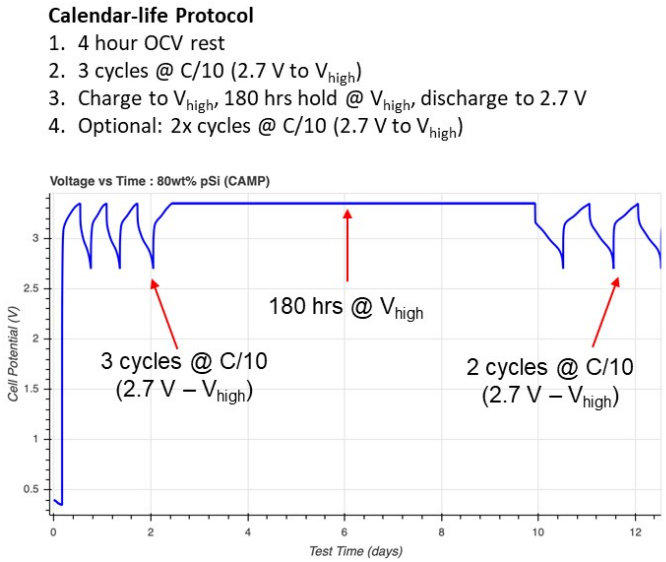

Figure 1. The test protocol to check the calendar life of Si-based cell. The cell couple is Paraclete Si 80% vs. an LFP cathode (CAMP)

The 180 h hold tests the stability of the Si SEI and evaluates the current magnitude over time with the premise that a stabilized passivated SEI should have a low leakage current. In **Figure 2**, a typical current response is shown wherein the current *diminishingly* flattens out after about 20 h of hold. This residual current is associated

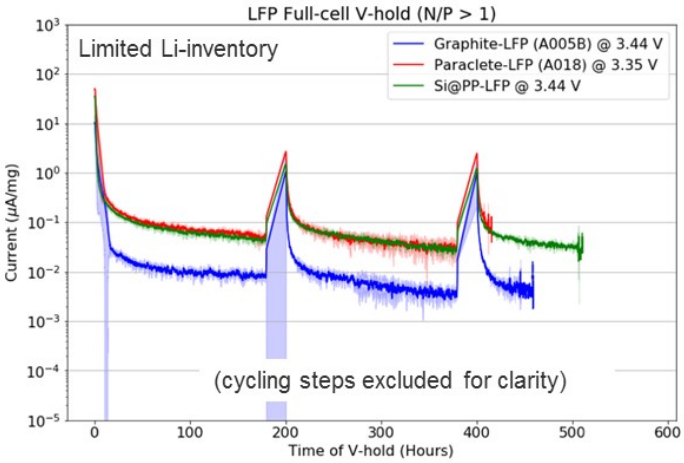

Figure 2. Current decay versus time upon voltage hold at 3.44 V (blue; graphite anode (10 mV vs. Li)), and 3.35 V (red and green curves; Si anode (100 mV vs. Li)).

with an unstable SEI whereby an irreversible electrochemical reaction of the Si (or at graphite) is occurring which is consuming lithium. Note that the graphite-LFP full cell (blue trace) has about an order of magnitude less current on long hold that indicates a good passivation on the electrode surface. The red and green traces are the Si-containing full cells; one with a modified Si nanoparticle surface (green), and another with a commercial Si product (Paraclete – red). These residual currents in the silicon-containing cells are about an

order of magnitude higher than the graphite-containing cells, consistent with parasitic electrochemical reactions occurring at those electrode surfaces. The passivation is not as complete on Si as that of graphite.Taking the current in time residuals under constant voltage hold, integrating the capacity and re-plotting as % irreversible capacity relative to delithiation capacity yields **Figure 3**.

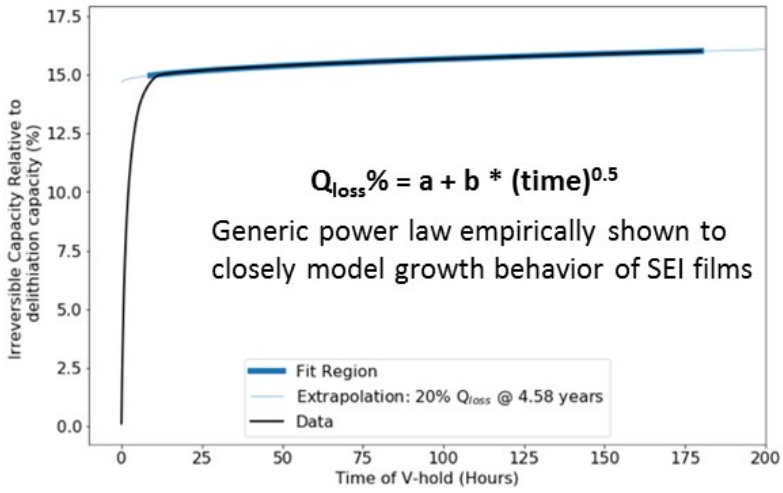

Figure 3. Full cell figure for a graphite-LFP cathode baseline chemistry. Plot of irreversible capacity relative to delithiation capacity percentage (%) over time. The inset contains an equation that fits the curve after the initial rise (< 10h; a=0 (reversible process) assumption) in irreversible capacity. Legend shows the raw data, the fit region, and the extrapolation to 20% charge lost over 4.58 years.

We have found that the curve in **Figure 3** can be empirically fit to a generic power law function with an 'a' term and a 'b' coefficient (fit value) times reciprocal 'time' or $Q_{loss}\% = a + b(time)^{0.5}$. This exponential fit in irreversible capacity is sufficient to extrapolate to multi-year timeframes. In this manner we can calculate when 20% loss in capacity occurs ($Q_{loss}\%$), which for the purpose of this example in **Figure 3** is 4.58 years. In this fit, the fast initial rise of the curve is neglected as we presume this feature is due to reversible lithiation.

The time window for the fit is also important for the lowest error. For example, in **Figure 4** we see the 180 h hold period shaded in green represents the preferred ~ 2 week data collection period, and the continuation of the fit to multiple hours is projected out in the unshaded portion. The goodness of fit is associated with the χ^2 value, with a good fit assigned when $\chi < 1$. Blue line is the fit from 1 to 180 h; orange from 30 to 180 h, and green from 100 to 180 h. The best fit to the power law equation is from 100 to 180 h, while the worst fit being from 1 to 180 h.

Using this methodology it is possible to make predictions on the calendar life of the Si material (or graphite as baseline) of interest. For example, if we use selected data on various cell chemistries we have tested thus far (Figure 5) it is apparent that the graphite-LFP cells are superior in their life as compared to the Si cases tested thus far. We will be moving to NMC cathodes for this analysis in the next round of experiments.

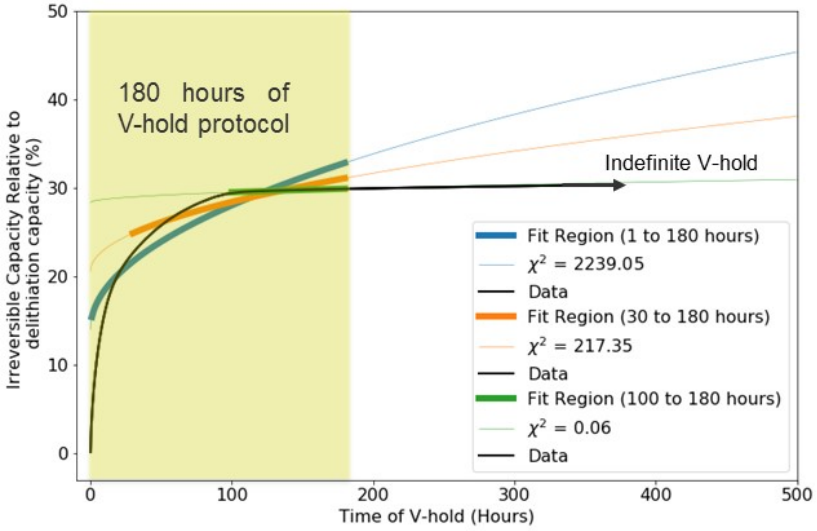

Figure 4. Percent (%) irreversible capacity relative to delithiation capacity versus time of voltage hold in hours for a Si-LFP full cell chemistry. The quality of the fits are shown in the legend with respect to the time range within 180 hours.

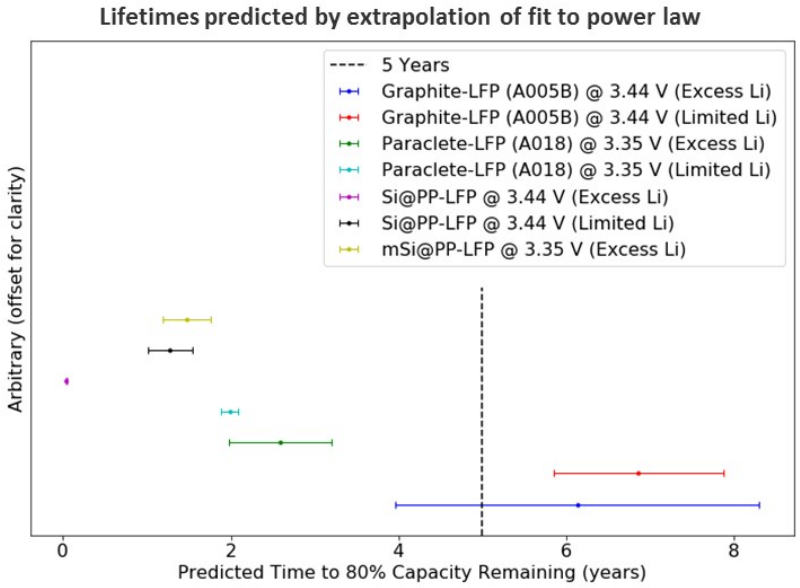

Figure 5. Cell lifetimes predicted by extrapolation of the constant voltage/current decay experiment. For example, the baseline graphite-LFP cells (red – limited Li; blue – excess Li) show longer projected calendar life than the Si-containing cells.

In the future work, we will be validating this approach by testing different n/p ratios, looking at multiple successive 180 h voltage holds, varying the testing temperature, and we will move to single-layer pouch (SLP) cells to boost the current signal for better fits with less noise.

Conclusions

A calendar life predictive model has been developed for Si-containing anodes using full cells based on either limited or excess Li supplied by LFP as cathode. The voltage is held for 180 h, and a power law equation has been fit to the percent of accumulated irreversible capacity relative to the reversible delithiation capacity. This irreversible capacity is likely associated with Li loss or trapping in the Si SEI. Based on the goodness of fit, we have been able to project a calendar life of the cell. We note that the type of chemistry (graphite vs. Si) of the full cell makes an impact as well as the voltage hold cutoff. The higher the voltage hold cutoff the shorter the lifetime of the cell as might be predicted for Si (higher vs. lower depth of charge). In addition, the amount of available Li (n/p ratio) can alter the lifetime of the cell.

Evaluation of Electrode Conductive Additives in Silicon Pouch Cells

Andrew Jansen, Steve Trask, Alison Dunlop (ANL)

Background

Numerous efforts in the CAMP Facility were directed to optimizing the silicon composite electrode with conductive additives, such as carbon black (*e.g.* Timcal C45), hard carbon, and graphite (flaky vs. round). In the case of Timcal C-45 carbon, the first cycle Coulombic efficiency of the C45 alone is only 62%, which is also similar to the hard carbon and flaky graphite (SFG-6-L). Another unfortunate side effect of many of these high surface area additives is that they require the use of additional binder to make a robust electrode. In the second quarter the CAMP Facility explored the idea of using inert conductive additives to replace all carbon-based additives. It is hoped that this approach could also enable the use of other binders, and perhaps better control the degree of electrode expansion. The following discussion is an update since the last quarter report.

In the second quarter, electrodes were designed with a concentration of 50 wt.% Si and 40 wt.% inert additive (B_4C, SiC, or SiO_2). Later, an additional boron carbide electrode was designed with 2 wt.% carbon black to create a baseline with higher electrical conductivity. These electrodes were made on the CAMP Facility's pilot-scale reverse-comma coater (A-Pro) with a target capacity near 2 mAh/cm^2. Coin cells were made with these electrodes first using lithium metal as the counter electrode and then NMC532 as the counter electrode - with "GenF" electrolyte (1.2 M $LiPF_6$ in EC:EMC (3:7 wt) +10 wt.% FEC). The half-cells were cycled 3 times at a C/20 rate between 1.5 and 0.01 V for formation, followed by rate tests between 1.5 and 0.05 V, then cycle life test at C/5 rate; all tests at 30°C. The full-cell coin-cells were tested using the Silicon Deep Dive test protocol (3x C/20, HPPC, C/3 cycling, HPPC, 3x C/20) in a voltage window of 3.0 to 4.1 V (GenF electrolyte, 30°C). It was apparent from these tests that the choice in conductive additive had little effect on the capacity utilization and retention during cycling.

Results

In the third quarter, the half-cell and full-cell coin cells were opened, along with other old silicon-based coin cells with similar cycling history and similar capacity loading (near 1.9 mAh/cm^2). The silicon electrodes were harvested, rinsed with DMC, and the thickness was measured. During the harvesting of many of these cells, it was observed that silicon-based anodes that experienced lithiation near or below 10 mV usually suffered from severe delamination – a situation that often occurred in half cell tests. This was especially true for anodes with high silicon content. Whereas, full cells were designed around a 50 or 100 mV lithiation cutoff, and reference electrode data indicates that the true lithiation potential is over 100 mV for majority of the cycle life. Table 1 is a compilation of the thicknesses of the pristine anodes and the harvested anodes (ones that did not show signs of delamination). The harvested (cycled) thicknesses shown in Table 1 are focused on anodes from full cells cycled for 100 cycles under the Si Deep Dive Protocol (100 cycles) between 3 - 4.1 V at 30°C, with similar n:p ratio.

While it is promising that the initial thickness of electrodes with inert additives (50 wt.% Si) are on par with the electrodes made with 80 wt.% Si, it is clear these cells still swell with cycling. On an optimistic note, the final thickness of the high silicon anodes is still half the thickness of the cycled graphite-only anodes. If the cycle life and calendar life problems can be solved, battery hardware can be designed to accommodate the swelling of the silicon-based cells – although the extra hardware needed will most likely lower the volumetric and mass-specific energy density (and probably increase cost).

Table 1 indicates that there is a dependence of anode swelling on silicon content. This was explored further by plotting the thickness increase (%) versus silicon content, which is shown in **Figure 1**. It was interesting to see a strong linear relationship exists between thickness increase and silicon content, despite the "minor" variations in particle size, morphology, capacity loadings, porosity, binders, and n:p ratio that occurs across these cells over the years. This was not a controlled study, but merely an effort to glean preliminary correlations from existing data. Ideally, this study needs to be redone in a controlled manner where all components are fixed and the counter

electrode is lithium metal, with lithiation of the silicon-based anode limited to a fixed voltage (*e.g.,* 100 mV) or capacity (*e.g.,* 1,000 mAh/g).

Table 1. Electrode Thickness of Variety of Pristine & Cycled Anode Electrodes made by the CAMP Facility

Negative Electrode from Full cells (3-4.1V, 100 cycles)	Initial thickness, calendered, µm	Cycled thickness, calendered, µm	% Increase
0% Si, 92% Graphite, 2% C45	41	44	7
5% Si, 83% Graphite, 2% C45	49	54	10
10% Si, 78% Graphite, 2% C45	33	41	24
15% Si, 73% Graphite, 2% C45	28		
30% Si, 58% Graphite, 2% C45	16		
50% Si, 40% B4C	11	21	91
50% Si, 40% B4C, 2% CB	12	20	67
50% Si, 40% SiC	11	21	91
50% Si, 40% SiO2	12	22	83
60% Si, 23% Graphite, 2% C45	18		
71% Si, 0% Graphite, 10% C45	9	20	122
80% Si, 0% Graphite, 10% C45	9		

Conclusions

In summary, it was determined that a new class of composite silicon electrodes made with inert additives such as semiconductor materials (B_4C, SiC) and insulators (SiO_2) performed surprisingly similar to silicon electrodes made with graphite and carbon black - despite the wide range of electrical resistivity. These electrodes were mechanically robust and had thicknesses almost identical to other high-silicon content electrodes. It is time to rethink the importance (or need) of carbon & graphite additives in silicon electrodes. Preliminary investigations also indicate that the anode thickness increase during cycling shows clear linear dependence on silicon content. Future efforts will consider other inert additives, variations in particle size, other binders, and new electrode architectures.

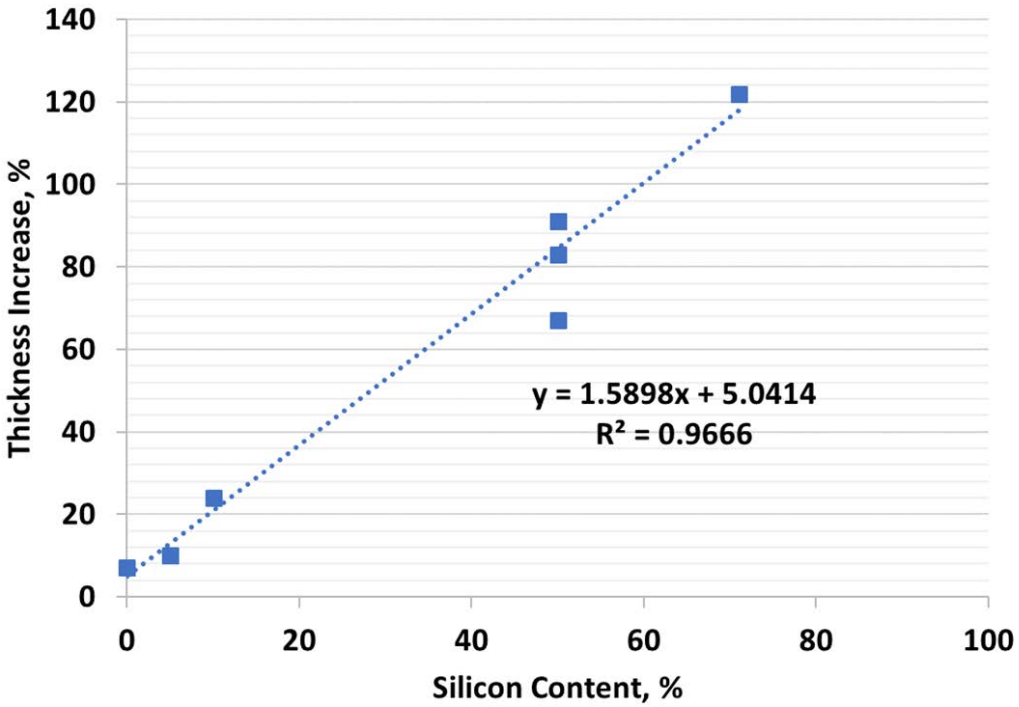

Figure 1. Thickness of harvested anodes from full cells cycled under Si Deep Dive Protocol as a function of silicon content.

Temperature Effect on SEI Formation and the Stability of Si Anodes (ANL)

Zhenzhen Yang, Minkyu Kim, Ira Bloom

Background

It is well known that temperature has a significant impact on the performance, safety and lifetime of lithium-ion batteries (LiB). However, the comprehensive effects of temperature on the SEI formation and stability have yet to be studied. Previously, we described the effect of temperature on the cycling performance of high-Si anodes in last report with and without 10wt% FEC additive in the Gen 2 electrolyte. In this quarter, we used XPS to investigate the SEI of these Li-Si cells within the temperature range of 25 °C to 55 °C. Little attention has been paid to the influence of temperature on the actual dynamic SEI growth and film properties. We used *in situ* electrochemical quartz crystal microbalance with dissipation (EQCM-D) to monitor SEI formation and properties in a time-resolved manner.

Results

Previously we discussed the cycling performance from Li-Si cells cycled in Gen 2 and Gen 2 + 10wt% FEC at various temperatures. We noted that, as the temperature increased from 25 ºC to 55 ºC, the cycle life decreased due to increased side reactions which consumes active Li^+ and increases as the temperature increases. In this quarter, we focused on the post-test analysis of Li-Si cells after the initial 5 cycles and compared the SEI properties at different temperatures with and without the FEC additive. **Figure 1** shows the XPS data from the cycled Si rich anodes within the temperature range we tested.

The C1s XPS spectrum of the surface consists of 5 signals after peak deconvolution at all temperatures in both electrolytes. The line at 284.8eV corresponds to aliphatic carbon (C-C). The signal at 286.6eV can be assigned to carbon atoms in one oxygen environment (C-O). Based on the binding energy, it is more likely to be consisted of carbon atoms bound to an electron withdrawing group, like R-C-OH (alcohols), R-C-O-C=O (esters) and C-O-COO (organic carbonate). Their presence is confirmed by the corresponding oxygen signals in the O1s spectrum. The peak at 287.8eV is assigned to a carbon atom doubly bound to one oxygen, as in ketones and aldehydes ($R_2C=O$, H-C=O) according to the literature. The peak at 289.6eV can be attributed to a carbon atom in a three-oxygen environment, such as Li_2CO_3 and organic carbonates. The signal at higher bonding energy, i.e., 290.5eV, might be related to the formation of polymeric fluoro-organic species (C_nF_m). The compound is also detected in the corresponding F 1s spectrum. Overall, based on the decomposition reactions in EC/EMC system, we can assume the assigned SEI components at Si surface (C-O-C, C-OH, C-O-C=O, $R_2C=O$, C-OC(=O)O and C_nF_m) are most likely to be polymeric. These organic units can be connected to form aliphatic chains, as indicated by a relative higher contribution of aliphatic carbons in the C1s spectrum. This is supported by the results that the trend with the contribution of CO_x species which is similar in O1s spectra as that in the C1s emission.

The F1s spectrum of the Si surface shows three peak positions in both electrolytes. The first line at 684.5eV is assigned to LiF, in agreement with most references. The peak appearing at 686.2eV can be attributed to $Li_xPO_yF_z$, based on the component assigned in the P2p spectra. The peak at

687.8eV is related to the formation of R-F (fluoro-organic species: C_nF_m, F-O-Si). XPS analysis shows the contribution of each component is quite different with/without the presence of FEC. SEI layer on anodes with FEC is primarily composed of LiF because the fluorinated ethylene carbonate (FEC) decomposes before EC and EMC. Overall, we can observe relatively less temperature-sensitivity of SEI chemistry in the Si-rich cell with FEC, implying the SEI is more stable with the additive.

Figure 2 shows the atomic percentage (at%) of the major SEI components, C, O, and F, on the Si surface that were calculated from XPS survey scans. The results clearly shows less carbonate (C, O) and more F species formed on the surface with FEC, confirming FEC can suppress EC/EMC decomposition to some extent at the first 5 cycles. It is interesting to note that surface content of C, O, and F increases as temperatures increases from 25°-45°C, but at 55°C, the values drop. This also is confirmed by lower peak intensity of C-O and C=O in C1s spectra in **Figure 1**, indicating fewer organic carbonates were formed at 55°C, particularly for the anode without FEC. In addition, there is an increase in fluorophosphates at this temperature. It might be due to the kinetics of SEI formation were enhanced and the partial decomposition of SEI components at this high temperature.

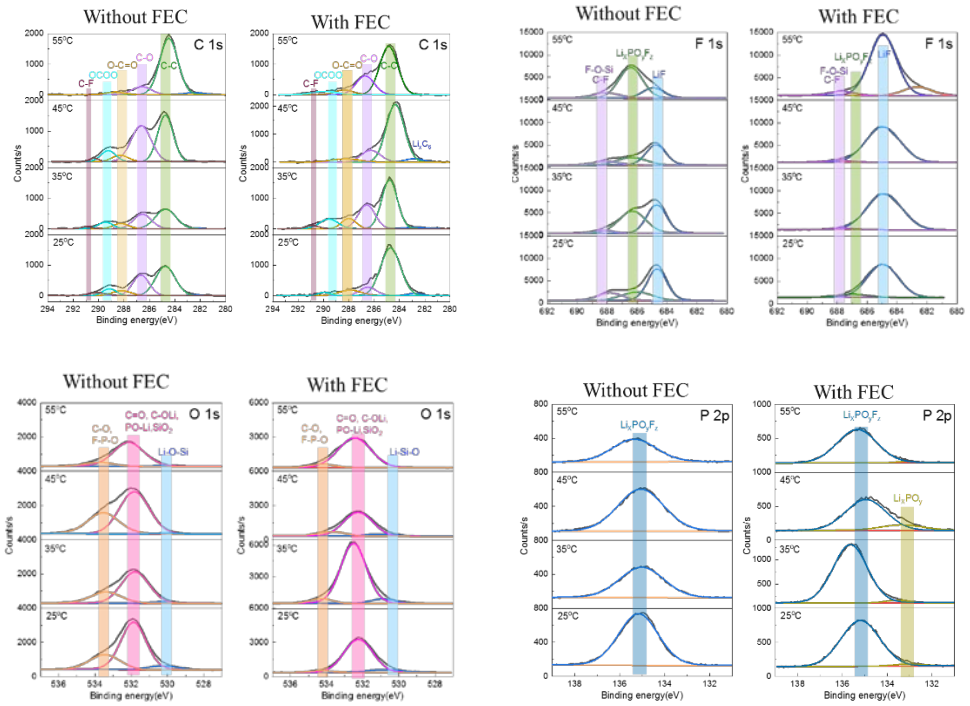

Figure 1. C1s, F1s, O 1s, and P2p XPS spectra of Si anodes after 5 cycles in the temperature range from 25 °C to 55 °C with and without 10 wt% FEC in Gen 2 electrolyte.

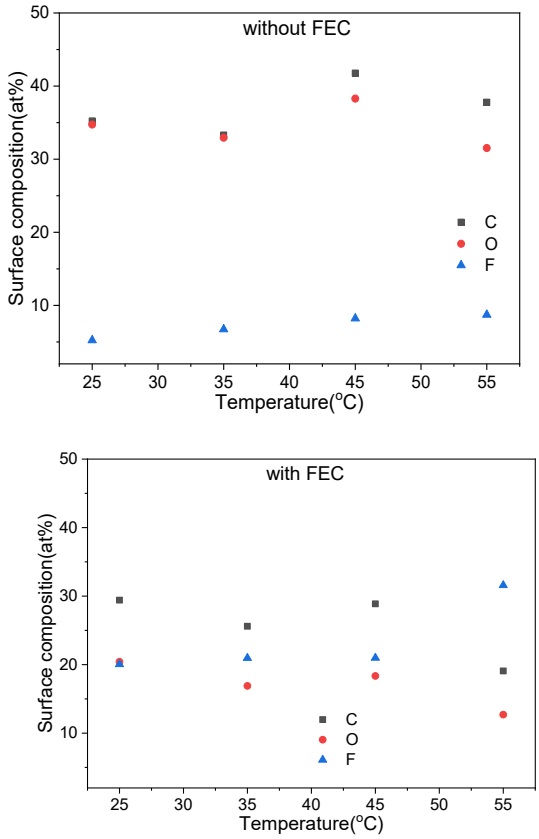

Figure 2. The atomic percentage (at%) of the major SEI components at the Si surface after 5 cycles in the temperature range from 25 °C to 55 °C with/without 10 wt% FEC in Gen 2 electrolyte.

In-situ electrochemical quartz crystal microbalance coupled with dissipation (EQCM-D) was employed to characterize SEI formation and changes, including changes in mass and mechanical properties, during the lithithiation/delithiation process on Si thin film electrodes. The change in mass on the electrode can be calculated based on the frequency change according to Sauerbrey equation. The advantage of EQCM-D in this work is that it uniquely measures a second parameter, energy dissipation (D) on the electrode, which is related to the properties of interfacial SEI films, such as rigidity and viscoelasticity that contribute to the measured frequency shifts. Surface film formation at different temperatures on Cu surface was investigated in the first step because Cu does not alloy with Li and Cu use allows us to focus on the influence of temperature on SEI. Our understanding the formation and chemistry of SEI is confounded by the significant volume change of Si during lithiation/delithiation. Thus, studying the SEI formation on Cu can provide us a better method to understand electrolyte decomposition behaviors with temperature change without any complications.

Figure 3 shows the preliminary results from cyclic voltammogram (CV) scans and *in-situ* EQCM-D measurement on Cu coated sensors with Gen 2 from 25ºC-45ºC. In the first CV sweep from open circuit potential (OCP, ~3.06 V) down to 0.01V, two small board reduction peaks were observed around 2.6 V and 2.0 V at 25ºC and 35ºC, indicating to the formation of passivating layer. While at 45ºC, a few small peaks were observed instead and became gradually larger (a broad shoulder) as compared to the curves at lower temperatures. The peak at ~2.0 V is attributed to reduction of the PF_6^- anion based on reports in the literature. Note that the current increases significantly below 0.2 V vs. Li/Li+, indicating that the Li plating is dominant below this potential. Two oxidation peaks were seen on the reverse scans at 0.15 and 0.25 V, signifying the oxidation (anodic stripping) of the deposited lithium. The passivating film formed by the reduction of electrolyte in the first cycle gave some protection to the Cu substrate and, thus, diminished the reduction current in subsequent cycles. In the three cells tested at different temperatures, the frequency or mass changes were different between the first scan and the following cycles, as shown in **Figure 3**b. In the first cycle from OCP-0.01V, where SEI formation mainly occurs, the mass increase was more than that of the other cycles. It decreases as temperature increased from 25 to 45ºC, as shown in **Figure 3**b (0~3600s). This trend continued after 5 cycles. During the positive scans, not all the mass due to Li plating stripped off from the electrode. As a result, the deposited mass and removed (or decomposed) mass for each cycle are not balanced at first five cycles. Some Li trapped in the surface film or associated with side reactions (probably via a non-electrochemical process) in the following cycles to form "dynamic and thick" SEI, resulting in, overall, continued mass increase after more cycles. The results also reveal more SEI species stay on electrode surface at lower temperatures. In the next step, same experiment will be carried out at 55ºC and will include the FEC additive. Moreover, the experiment will be repeated to obtain conclusive results.

In addition, a 100-nm-thick Si thin film was coated on Cu substrate and tested in EQCM cells with Gen 2 and Gen 2+10 wt% FEC electrolytes at 25ºC. **Figure 4** displays the preliminary results. Based on the mass change, we find that the initial SEI formation process is slow before Li reactions with silicon (>0.5V) but increases significantly from 0.5-0.01V in both electrolytes. But the total mass after Li delithiation in Gen 2 is more than that in FEC cell, indicating FEC can reduce the electrolyte decomposition and formation of the SEI on Si surface. It is noteworthy that the *D* values, which represent film rigidity, also change associated with mass change within one-cycle discharge/charge. More specifically, *D* increases upon Li insertion and remains high upon Li removal, indicating the structure of the formed SEI became viscoelastic due to Li reactions with Si. Furthermore, the smaller *D* value means that the film formed on Si surface is more rigid when FEC is present. In the next quarter, we will continue studying the temperature effect on SEI formation and stability on Si thin film surface by EQCM-D.

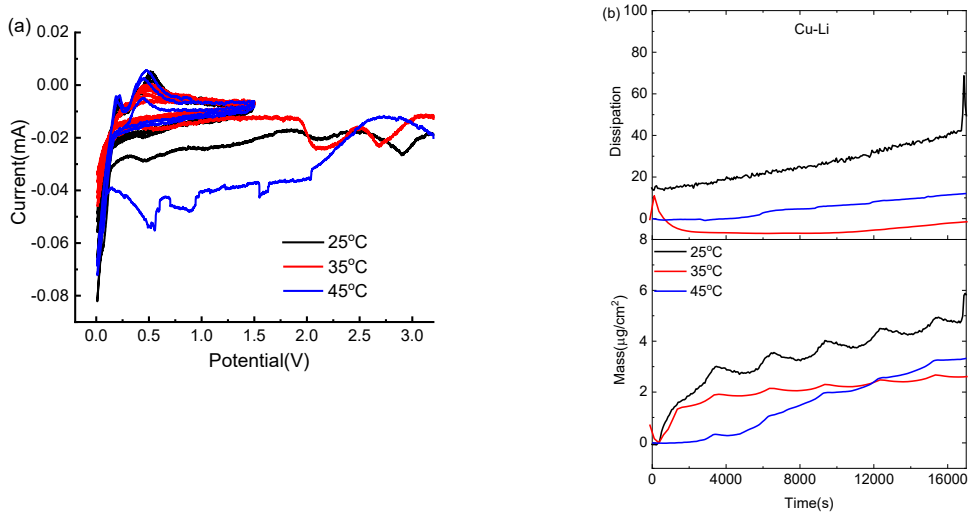

Figure 3. (a) Cyclic voltammogram of EQCM-D cells with Cu-coated quartz sensor as working electrode; Li metal foil as counter/reference electrode; and Gen 2 as electrolyte. The voltage was swept from OCP down to 0.01V and then scanned between 0.01V-1.5V vs. Li/Li+ at a rate of 1 mV/s. (b) Time dependence of the EQCM-D parameters, mass change and energy dissipation shifts, ΔD_n, during the first five CV cycles obtained on Cu surface in Gen 2 electrolyte at different temperatures.

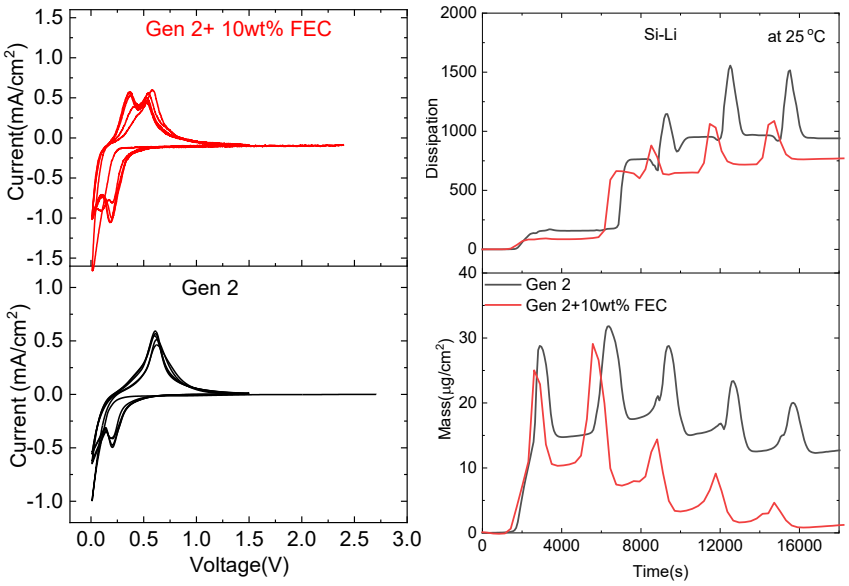

Figure 4. (a) Cyclic voltammograms of the first five cycles of the Si electrode from OCP (~2.8 V) to 0.01 V and then between 0.01-1.5V in Gen 2 electrolyte and with 10 wt% FEC. Scan rate: 1 mV/s. (b) Simultaneously recorded EQCM-D mass change and energy dissipation shifts, during the first five CV cycles.

Conclusions

SEI formation and stability with and without FEC additive at different temperatures was investigated in high-Si half cells by XPS. The XPS results show that different chemical species of SEI formed in the FEC-containing cells. Fewer organic species and more LiF was observed in Si-rich cells with FEC addition. As result, cells with FEC showed relatively less temperature-sensitivity of SEI chemistry when compared to the cells in Gen 2 only. SEI formation and changes as a function of temperature was also explored by *in-situ* EQCM-D analysis. The SEI layer formed on Cu electrodes exhibits a dynamic behavior at the tested temperatures. It forms rapidly during the first negative scan, and, on subsequent cycling, it continued to increase after removal of part of Li in Gen 2 electrolytes. The dissipation indicates that the rigidity of the film also changed with cycling. The quantitative mechanical properties, including the shear elastic modulus and shear viscosity, will be determined after more confirmed data are obtained.

Binder and Mechanical Stability Studies on Silicon Electrodes (NREL)

Trevor Martin, Ryan Pekarek, Kae Fink, Jaclyn Coyle, Nathan Neale (NREL)

Background

NRELs focus has been evaluating the relationship between the chemistry at the silicon surface and the polymer binder to understand which silicon surface chemistry/binder interactions stabilize the silicon particles toward cracking. NREL has been investigating PAA-based binders with a variety of surface chemistries (e.g., SiO_x, SiH_x, molecular silanes) on model wafer systems and correlate the degree of binding strength with the cycling performance of identical surface chemistry/binders on silicon nanoparticle (Si NP)-based electrodes. The Q3 Milestone (NREL) is to assess the silicon surface chemistry/binder combinations as a function of binder deposition solvent and drying temperature.

Results

Laboratory activities were wound down to zero for this project before the end of Q2 (3/19/20), with activities slowly ramping back up in June 2020. We have been working toward this Q3 Milestone by performing mechanical adhesion and electrochemical studies on various percentages of esterified PAA binder with a single solvent (water) and temperature (120 °C). The ~150 nm diameter Paraclete Si NP samples obtained from CAMP only achieve reasonable performance in composite electrodes when processed in water, which obviates the need to explore additional solvents. Additional work on at least one additional temperature 150 °C, which is the drying temperature from optimized CAMP process, will be explored to achieve the Q3 Milestone – deferred to Q4 owing to the SARS-CoV-2 pandemic.

In Q2FY20 we were able to utilize our Cantilever Beam Test (CBT) technique to probe how the bond strength between PAA and Si surfaces (both SiH_x and SiO_x surface termination) correlates to the electrochemical performance of 3D composite electrodes. Specifically, we were able to show that esterified polyacrylic acid (E-PAA) materials, synthesized at NREL, exhibit a systematic decrease in bonding energy as the amount of esterification increases, which was consistent with our hypotheses. We were also able to demonstrate that PAA bonds more strongly to SiO_x-terminated surfaces than to SiH_x-terminated surfaces, which was also consistent with our hypothesis and which helped explain some of our electrode cycling results.

In Q3FY20 we used tensile stress measurements to analyze the mechanical properties of Paraclete A018 and C65 based composite electrodes with three different amounts of esterification in the PAA binder of aqueous-based slurries comprised of 80 wt% Paraclete, 10 wt% C65, and 10 wt% E-PAA. **Figure 1** shows the data from these initial tests, where the copper foil current collectors were coated with the electrode slurry, dried at 120 °C, cut to size, and placed in a mechanical testing system for subsequent tensile analysis.

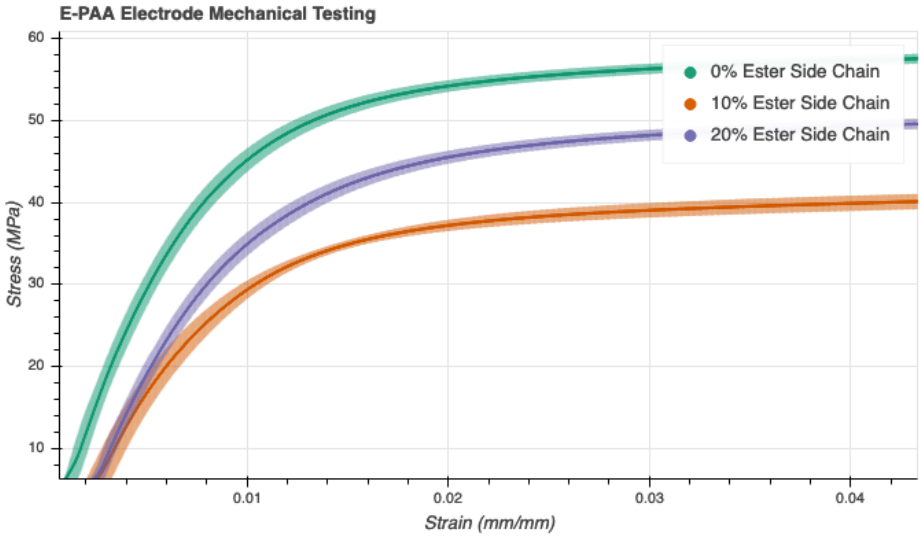

Figure 1. Mechanical properties of Esterified PAA (E-PAA) silicon electrodes. Data were collected by measuring the tensile stress of electrodes coated on copper foil.

The data show that there is *no observable* trend between stress and the degree of esterification measured between the electrode coated copper foil. This is likely due to the fact that the mechanical properties of this system are largely dominated by the properties of the copper foil and because the electrode films only have a minute impact on the bulk mechanical properties of the assembly. Therefore, it is likely that these data are mostly only probing the mechanical properties of the copper foil.

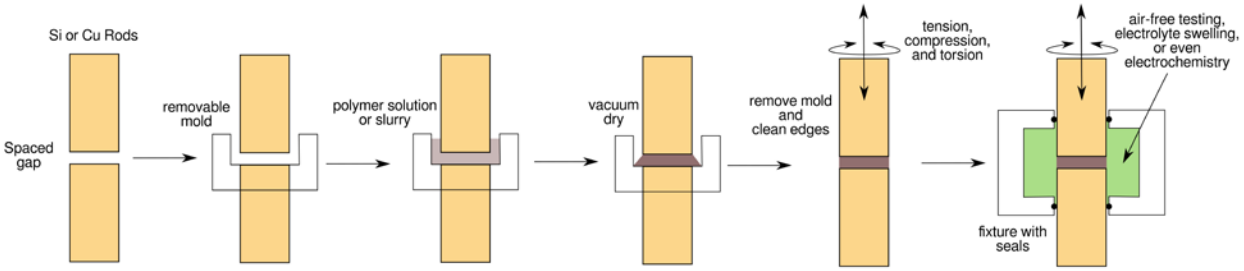

Figure 2. Procedure for testing the mechanical properties of electrode materials using the new experimental design.

In order to better address these issues, we spend significant time in the work-from-home period during Q3 developing a new system for directly testing the mechanical properties of binder films and electrode composites when coated onto either silicon or metal current collector substrates. The details of this experimental design are illustrated in Figure 2, and Figure 3 details the design of the experimental apparatus. We are currently fabricating the experimental apparatus for these tests and we will begin to collect initial data during Q4FY20. Importantly, we believe that this method will potentially allow us to conduct experiments that examine the mechanical properties of binders or electrodes with concurrent exposure to electrolyte or even potentially during cycling.

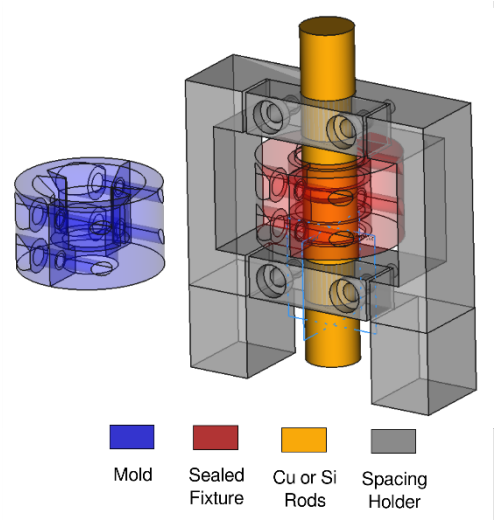

Figure 3. Design of apparatus for future mechanical experiments

Despite this result, we have made major progress toward achieving the Si Deep Dive Q3 Milestones. In Q3, we developed a technique to collect FTIR spectra under binder drying conditions that allows us to investigate the temperature-dependent chemistry of the E-PAA and correlate these data with our mechanical and electrochemical results. In this new experiment, we place the aqueous E-PAA solution on a diamond ATR prism in a custom-built cell. We place the cell under vacuum (~20 mTorr) and collect spectra while heating the diamond. This setup replicates slurry drying conditions used to dry 3D composite electrodes and therefore provides chemical information on changes to the Si-binder chemistry during this process. Our experimental matrix included two temperature-controlled experiments using E-PAA binders with three degrees of esterification (0% – i.e., 100% PAA – 25% and 50% ester sidechain, as described above). In the first experiment, spectra were collected while the temperature was increased from 25 to 100 ºC. In the second experiment, spectra were collected while the E-PAA was held at 100 ºC over 24 h. These data are shown in **Figure 4**. We have made two key observations using this technique:

1) *Esterification alters the conformation of the polymer, increasing stability*
   The C=O region (1800–1600 cm^{-1}) contains two positive peaks. The higher wavenumber peak is a *cis* conformation where the polymer sidechains are in close proximity while the lower wavenumber *trans* peak corresponds to a conformation where the sidechains are on opposite sides of the polymer backbone. Esterification dramatically increases the size of the sidechain and therefore sterically favors the *trans* conformation. Accordingly, we observe more *trans* conformation in the ramping temperature experiment as the degree of esterification increases. Interestingly, over 24 h at 100 ºC the *cis* peak decreases without a commensurate increase of the *trans* conformation, suggesting the *cis* conformation reacts preferentially, giving a different chemical product. The 50% polymer shows remarkable stability during the 24 h experiment. Notably, we do not observe anhydride features.

2) *PAA crosslinking occurs via Esterification decreases crosslinking*
   In the C–O region (1000–1400 cm^{-1}) we observe several peaks assigned to ester, ketone, or ether groups that increase during the temperature ramp. As expected, E-PAA shows an increase in the peaks characteristic of ester moieties (~1140 and 1100 cm^{-1}). 100% PAA also contains some ester groups to a lesser extent, likely a product of polymer crosslinking. No further changes is observed in these groups over the 24 h hold at 100 ºC. Another predominant product of crosslinking reactions, an ether, is hindered by esterification. This reaction is slower, predominantly observed during the 100 ºC hold, and is inversely proportional to the degree of esterification. Considering these observations and those mentioned above, the predominant

reaction of PAA during vacuum drying appears to be reaction of 2 *cis* carboxylic acids (–COOH) to form 1 ether linkage (C–O–C) via decarboxylation and dehydration.

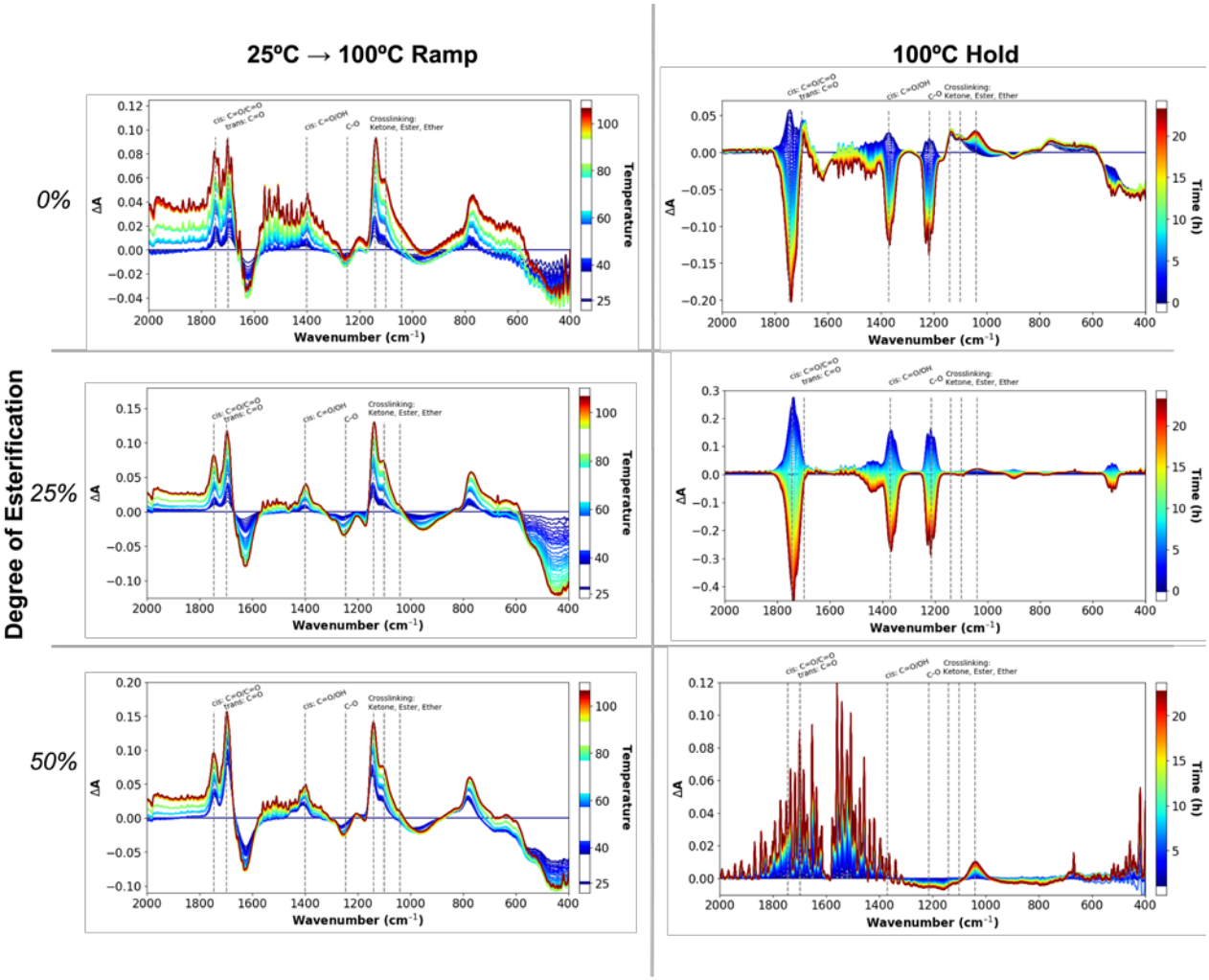

Figure 4. Temperature-dependent FTIR measurement of the esterified polyacrylic acid (E-PAA) binder drying. The left panels show the spectra while heating from 25 ºC to 100 ºC while the right panels depict spectra while holding at 100ºC for 24 hours. The top, middle, and bottom panels correspond to 0, 25 and 50% ester sidechain, respectively. The first spectrum (25ºC, atmospheric pressure) is subtracted from each spectrum to produce the difference spectra shown.

This newly identified PAA reactivity under drying conditions has major ramifications for the binding strength to Si surfaces as well as the mechanical properties of composite electrodes. We hypothesize that similar reactivity between Si–OH groups that terminate SiO_2 surfaces, prevalent in most Si NP samples including Paraclete, results in similar reactivity to give silyl ether moieties, *Si–O–CR_3 (where *Si denotes a surface Si atom). These chemical functionalities were previously identified by our team[1] as being stable toward chemical degradation in Gen2 electrolyte and may offer insight into why PAA and its derivatives appear to work well with Si-based active materials.

Conclusions

In Q3FY20 we determined that future mechanical testing will need to directly measure the mechanical properties of binders and electrodes. Thus, we will need to measure shear and adhesion strength as well as compression and tension. In addition, these experiments will need to be adaptable to a variety of testing conditions including exposure to electrolyte and will need to be directly relatable to electrochemical and spectroscopic analysis. Accordingly, we have worked to develop a new experimental apparatus that can be used to achieve these goals. During Q3FY20 we also dedicated significant effort to developing a new method to study the chemical changes that occur in binders during the electrode drying process via an in-situ FTIR method. We were able to see evidence that the electrode drying process even at modest temperatures as low as 100 °C changes the final structure of the binder to form ether cross-linkages, not anhydrides, derived from *cis* carboxylic acid groups. It is possible to reduce the degree of crosslinking present in the dried polymers by converting a portion of the carboxylic acids to esters via esterification.

We are currently conducting electrochemical experiments to study the cycle and calendar lifetime of 3D composite electrodes performance using the same ratios of E-PAA binder. These experiments will directly correlate the electrochemical performance with the binding strength between the active Si material and the polymer to achieve the Q3 Milestone. Furthermore, we are also conducting spectroelectrochemical measurements on these electrodes to examine how the degree of esterification impacts reactions with electrolyte via in-situ ATR-FTIR spectroscopy.

In Q4FY20 we will combine these new methodologies to study how the degree of esterification impacts the mechanical properties of the polymers and electrodes, how esterification impacts reaction with electrolyte, and whether these data relate to cycling and calendar life performance.

References

[1] "Intrinsic Reactivity of Solid-Electrolyte Interphase Components in Silicon-Lithium Alloy Anode Batteries Probed by FTIR Spectroscopy," R. T. Pekarek, A. Affolter, L. L. Baranowski, J. Coyle, T. Hou, E. Sivonxay, B. A. Smith, R. D. McAuliffe, K. A. Persson, B. Key, C. Apblett, G. M. Veith, N. R. Neale, *Journal of Materials Chemistry A*, **8**, 7897–7906 (2020). https://doi.org/10.1039/C9TA13535A

Probing Clustering Dynamics of Li-PAA using Rheology Coupled Ultra-Small Angle Neutron Scattering (USANS)

Mary K. Burdette-Trofimov (ORNL), Beth L. Armstrong (ORNL), Ryan Murphy (NIST), Markus Bleuel (NIST), Paul Butler (NIST), Alexander Rogers (ORNL), Gabriel Veith (ORNL)

Background

Based on the previous x-ray nanotomography images of silicon anodes fabricated with cesiated poly(acrylic acid) (CsPAA) and rheology coupled ultra-small angle neutron scattering (rheo-USANS) experiments on poly(acrylic acid) based silicon slurries[1], it has become apparent that electrode architecture is key in developing silicon anodes with extended calendar life. Interestingly, the rheo-USANS of silicon slurries fabricated with lithiated poly(acrylic acid) (LiPAA) shows that the aggregation/agglomeration behavior (i.e. clustering dynamics) in the slurry can be used to predict the electrode architecture at various casting shear rates or wet gaps. Herein, the aggregation/agglomeration behavior of silicon slurries made with LiPAA is investigated with and without dispersant being present in the slurry.

Results

USANS was utilized to probe the aggregation (length scale of 300-1000 nm) and agglomeration (length scale of 1 μm-10 μm)[2-5] of silicon slurries fabricated with 450k g/mol LiPAA (Si+LiPAA) with and without dispersant, an 1.8k g/mol LiPAA for four different shear rates: 0 Hz, 30 Hz, 200 Hz, and 500 Hz. Each of these shear rates was chosen to reflect a shear rate the slurry would be exposed to on the coated used at the CAMP facility at Argonne National Laboratory. Specifically, 0 Hz represents the slurry at rest after mixing; 30 Hz represents the slurry being fed gravitationally from the hopper to the doctor blade; 200 Hz represents a slurry being cast with a wet gap of 45 μm, and 500 Hz represents a slurry being cast with a wet gap of 15 μm. **Figure 1** presents neutron scattering intensity plotted as a function of Q, the neutron wave vector, which is a length scale in reciprocal space. From **Figure 1**, it can be noticed that the USANS curves of Si+LiPAA with and without dispersant at 0 Hz and 30 Hz are fairly similar, indicating that dispersant does not have a great effect on aggregation/agglomeration on the Si+LiPAA slurry at these shear rates. However, the USANS curves of the samples at 200 Hz and 500 Hz look different from one another, indicating that dispersant has more of an effect on Si+LiPAA at those shear rates. More specifically, at 0 Hz, the aggregation of Si+LiPAA with and without dispersant is at exactly the same level. This indicates that the dispersant is not cleaving silicon aggregates, which means that the dispersant is likely not the right length to overcome the hydrodynamic forces in the slurry.[6-9] At 30 Hz, aggregation increases for both Si+LiPAA with and without dispersant, but aggregation increases more for Si+LiPAA with dispersant than without dispersant (from 0 Hz to 30 Hz aggregation increases by 2.7 times and 4 times for Si+LiPAA without and with dispersant respectively). This may indicate that the dispersant is acting like a tether to multiple polymer chains, causing an increase in aggregation behavior. As shear rate approaches 200 Hz and 500 Hz, aggregation decreases, but only the Si+LiPAA slurry without dispersant achieves an aggregation level below the aggregation level at 0 Hz and does so only at 500 Hz. Therefore, it is likely that an Si+LiPAA slurry made with dispersant will result in less homogeneous electrode. From x-ray tomography data, adding dispersant to Si+CsPAA slurries caused the electrode to be more homogeneous laterally, but drove the silicon intermixed with binder areas deeper into the electrode, making them less homogeneous throughout the thickness of the electrode (See **Figure 2**). In addition, a Si+LiPAA slurry made without dispersant would likely need to be cast at a rate of at least 500 Hz to break up agglomerates to achieve an electrode with the smallest amount of aggregation, which would likely lead to a more homogeneous electrode architecture. The Si+LiPAA slurries, together, show that LiPAA may be making a hard sphere of agglomerated polymer on silicon aggregates. This would likely not lead to a cohesive network of silicon in a polymer matrix, leading to an inhomogeneous electrode with poor calendar life.

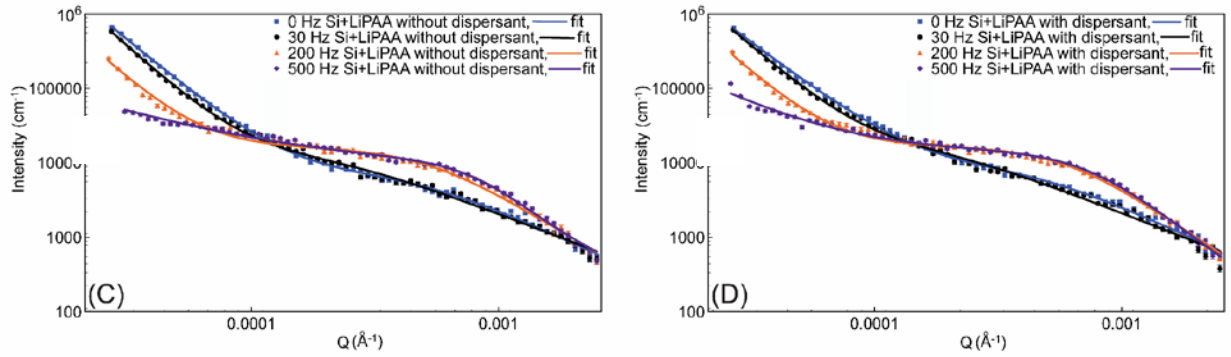

Figure 1. USANS data of (left) Si+LiPAA solution in D_2O without dispersant and (right) Si+LiPAA solution in D_2O with 1,800 g/mol LiPAA dispersant plotted as intensity of the scattered beam as a function of Q, which is a length scale in reciprocal space. USANS measurements performed at 0 Hz are represented by blue squares, 30 Hz are represented by black circles, 200 Hz are represented by orange triangles, and 500 Hz are represented by purple diamonds. The blue, black, orange, and purple lines represent the fit of the correlation length model to the data at 0, 30 Hz, 200 Hz, and 500 Hz, respectively. There are error bars on all points; however, some error bars are smaller than the points.

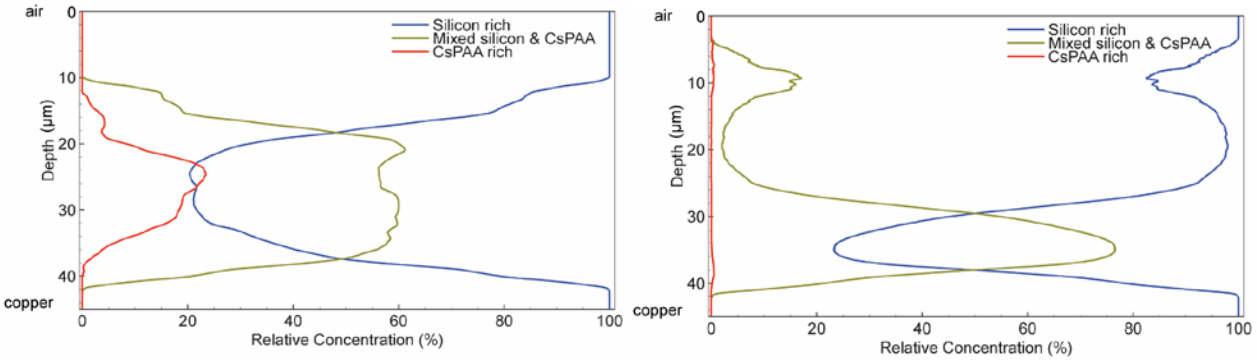

Figure 2. Relative concentration of silicon-rich/CsPAA binder poor regions (blue), intermixed silicon and CsPAA binder regions (yellow), and CsPAA binder rich/silicon-poor (red) as a function of depth in the electrode where the two extremes are at the electrode-air interface and at the silicon-copper interface for electrodes made with (left) CsPAA without dispersant, and (right) PCM CsPAA with dispersant.

Conclusions

LiPAA is often used over PAA because it raises the viscosity of the slurry, which may reduce sedimentation. However, this rheo-USANS data makes it clear that LiPAA is having far reaching implications on the aggregation behavior of the slurry, which will likely directly affect the homogeneity of the resulting electrode.

References

1. Burdette-Trofimov, M. K.; Armstrong, B. L.; Rogers, A. M.; Heroux, L.; Doucet, M.; Yang, G.; Phillip, N. D.; Kidder, M. K.; Veith, G. M., Understanding Binder-Silicon Interactions during Slurry Processing. *J. Phys. Chem. C* **2020,** *124* (24), 13479-13494.
2. Agamalian, M.; Alamo, R. G.; Kim, M. H.; Londono, J. D.; Mandelkern, L.; Wignall, G. D., Phase behavior of blends of linear and branched polyethylenes on micron length scales via ultra-small-angle neutron scattering. *Macromolecules* **1999,** *32* (9), 3093-3096.
3. Agamalian, M.; Heroux, L.; Littrell, K. C.; Carpenter, J. M.; Iop, Progress on The Time-of-Flight Ultra Small Angle Neutron Scattering Instrument at SNS. In *22nd Meeting of the International Collaboration on Advanced Neutron Sources*, 2018; Vol. 1021.
4. Hammouda, B., Solvation characteristics of a model water-soluble polymer. *Journal of Polymer Science Part B-Polymer Physics* **2006,** *44* (22), 3195-3199.
5. Hammouda, B.; Ho, D. L.; Kline, S., Insight into clustering in poly(ethylene oxide) solutions. *Macromolecules* **2004,** *37* (18), 6932-6937.
6. Li, C. C.; Lee, J. T.; Peng, X. W., Improvements of dispersion homogeneity and cell performance of aqueous-processed LiCoO2 cathodes by using dispersant of PAA-NH4. *J. Electrochem. Soc.* **2006,** *153* (5), A809-A815.
7. Li, J. L.; Armstrong, B. L.; Daniel, C.; Kiggans, J.; Wood, D. L., Optimization of multicomponent aqueous suspensions of lithium iron phosphate (LiFePO4) nanoparticles and carbon black for lithium-ion battery cathodes. *J. Colloid Interface Sci.* **2013,** *405*, 118-124.
8. Li, J. L.; Armstrong, B. L.; Kiggans, J.; Daniel, C.; Wood, D. L., Optimization of $LiFePO_4$ Nanoparticle Suspensions with Polyethyleneimine for Aqueous Processing. *Langmuir* **2012,** *28* (8), 3783-3790.
9. Li, J. L.; Armstrong, B. L.; Kiggans, J.; Daniel, C.; Wood, D. L., Lithium Ion Cell Performance Enhancement Using Aqueous $LiFePO_4$ Cathode Dispersions and Polyethyleneimine Dispersant. *J. Electrochem. Soc.* **2013,** *160* (2), A201-A206.

Materials Studies

LHCE Electrolytes for Silicon - Containing Anodes (PNNL)

Ji-Guang Zhang, Xiaolin Li

Background

Nanoscale silicon has been widely used to avoid pulverization of silicon particles during cycling process. However, the large surface area of nanoscale silicon or micron sized porous silicon also leads to a continuous reaction between lithiated silicon and electrolyte which may lead to continuous growth of SEI layer and increasing cell impedance. Another possible degradation mechanism involves the cross talk phenomenon where cathode cations dissolve from the surface and precipitate on the anode. The migration of dissolved Mn from the cathode may poison silicon or silicon SEI at the anode, as has been seen in graphitic systems. Additionally the commonly used FEC additive, which is highly effective in forming a stable SEI layer on silicon, may form a detrimental cathode electrolyte interface (CEI) on cathode surface leading to impedance increase. Therefore, minimize the surface area of silicon and identifying a stable electrolyte are critical for long term stability of silicon based Li-ion batteries.

In this project, we seek to develop new approaches to extend the cycle life and calendar life of silicon containing Li-ion batteries by designing a stable porous silicon structure and a stable electrolyte to improve the mechanical strength and ionic conductivity of SEI layer. Micron sized silicon particles with nano-porosity and protected by effective carbon coating will be developed and evaluated to evaluate the interaction between cycled silicon and electrolytes. The degradation mechanism of silicon anodes during shelf storage will also be systematically investigated to enable high energy Li-ion battery with Si-based anodes and increase market penetration of EVs and PHEVs.

Results

In this quarter, we continued to develop our LiFSI-DMC-based Locally High Concentration Electrolytes (LHCE) and demonstrated that 1H,1H,5H-Octafluoropentyl 1,1,2,2-Tetrafluoroethyl Ether (OTE) as a new diluent. OTE has large molecular weight compared to bis(2,2,2-trifluoroethyl) ether (BTFE) or 1,1,2,2-tetrafluoroethyl-2,2,3,3-tetrafluoropropyl ether (TTE), thus gives higher boiling point (133 ºC). As the intrinsic low boiling point and volatility of BTFE and TTE (62 ºC and 93.2 ºC, respectively) have potential disadvantage in battery manufacturing process or battery performance at elevated temperatures, OTE-based LHCE (designated: Lc) potentially can have great importance towards practical applications. We systematically adjusted the electrolyte salt concentration and the solvent-to-diluent ratio. **Figure 1**a show the salt concentrations of various electrolyte before dilution. They are set at 3 concentrations of 3.7M, 4.5M, and 6.2M. **Figure 1**b shows the solvent-to-diluent (OTE/DMC) ratio, which is adjusted from 3 to 0.25 for various electrolytes. The Lc electrolytes of extremely high concentration of 6.2M before dilution (Lc8, Lc9, and Lc10) precipitate salt after the addition of OTE diluent. The rest of the Lc electrolytes have concentrations from 0.62M (Lc1) to 3.12M (Lc7) after dilution, as shown in **Figure 1**c.

All seven Lc electrolytes (Lc1 to Lc7) are tested in NMC532||Si/Gr coin full cells at 30 ºC (**Figure 2**). The testing protocol is similar with previous quarter report. The composition of anode is 88 wt% Si/Gr composite (BTR New Energy Materials Inc.), 10 wt% polyimide (P84, HP POLYMER GmbH) and 2 wt% carbon black (C65, Imerys). The anode loading level is 2.7 mg/cm^2. The composition of cathode is 90 wt% Li[$Ni_{0.5}Mn_{0.3}Co_{0.2}$]O_2 (NMC532, Toda), 5 wt% carbon black (C45, Imerys), and 5 wt% polyvinylidene fluoride (Solef 5130, Solvay). The loading level of each anode and cathode is adequately controlled to have the full cell N/P ratio of ~1.2. The anode was pre-cycled 3 times in the 2032 coin-type half-cell at a C-rate of 0.1C (=100 mA/g) and disassembled for full-cell assembly. The operational voltage window for pre-cycling is 0.02 V to 1.5 V. The full-cell was cycled for 3 cycles at the C-rate of 0.05C (based on cathode), then further cycled at the C-rate of 0.33C. The voltage window is between 3.0 V to 4.1 V.

Figure 2 shows the cycling performance of NMC532||Si/Gr full cells with various Lc electrolytes. At low salt concentration of 3.7M in DMC, the NMC532||Si/Gr full cell show improved capacity retention as the amount of diluent in Lc electrolyte decreases from Lc1 to Lc4. For Lc5, Lc6 and Lc7 with high salt concentration of 4.5M in DMC, the capacity retention decreases with further addition of OTE. The capacity retention in Lc5, Lc6, and

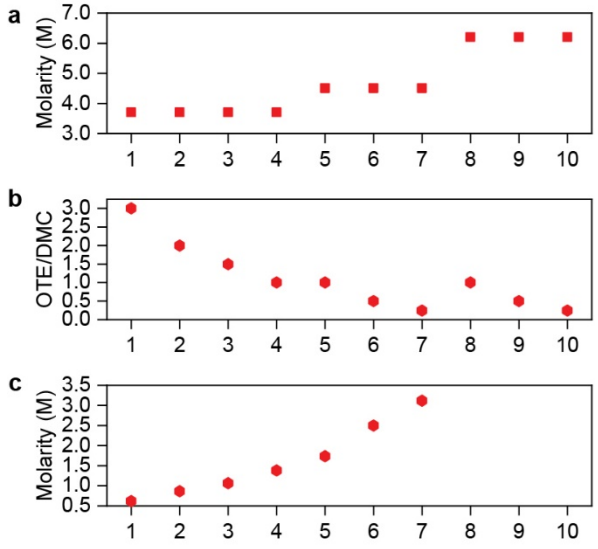

Figure 1. Systematical preparation of various Lc electrolytes. a, Initial salt molarity of HCEs. b, The ratio between OTE and DMC. c, Final salt molarity of various Lc electrolytes.

Lc7 over 250 cycles is ~91.2%. 92.5%, and 87.7%, respectively. The cell in Lc5 exhibits the best cycling stability. It is believed that adequate salt concentration and appropriate amount of diluent are critical for achieving an optimized cycle life. Excess amounts of OTE gradually deteriorates the cyclability because large molecular size of OTE may disturb Li ion transportation when the salt and solvent decompose during cycling. The optimized Lc electrolyte (Lc5) shows ~20% higher capacity retention at 250th cycle than that of Gen2 + 10% FEC electrolyte. It also has high coulombic efficiencies (CEs), among various Lc electrolyte and compared to baseline electrolyte (**Figure 3**). A close examination shows that the CE of the cells with Lc electrolyte increase rapidly in the first 10 cycles and stabilize >99.7%. It is consistent with the capacity retention improvement in **Figure 2**. Further investigation on the fundamental mechanism of how Lc electrolyte enables high performance Si anodes is undergoing.

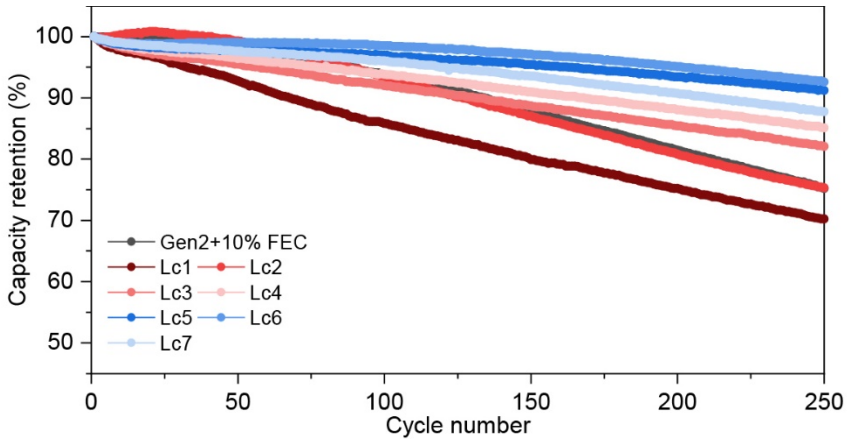

Figure 2. Capacity retention of NMC532||Si/Gr full cells cycled between 3-4.1V in various Lc electrolytes.

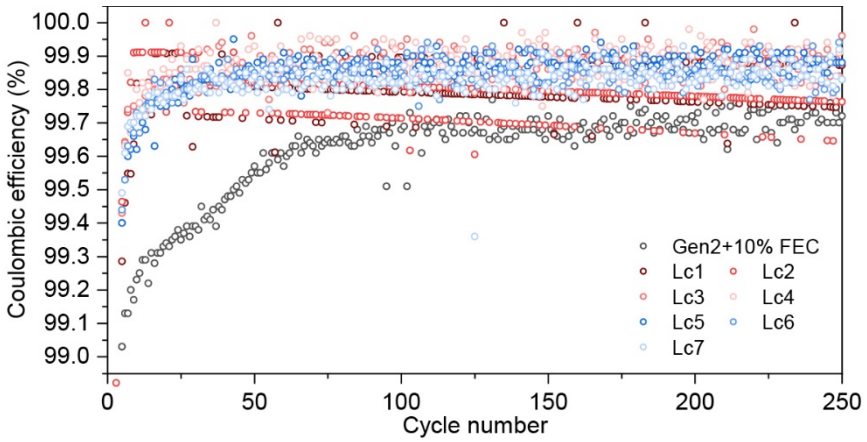

Figure 3. Coulombic efficiency of NMC532||Si/Gr full cells with different Lc electrolytes.

Conclusions

Locally high concentration electrolytes (LHCE) are an LIB electrolyte system based on LiFSI in a DMC solvent that has a non-interacting fluorinated solvent added to decrease the amount of free solvent available in the cell. The identification of free solvent has been seen as a source of reactivity in the cell. For LHCE studies here, the DMC solvent is diluted by a variety of fluoroethers (i.e. OTE, BTFE, TTE)) as the diluent. OTE has been identified to greatly improve the cycling stability of Si anodes. Full cell of NMC532||Si/Gr full cells with Lc5 electrolyte shows 91% retention over 250 cycles with CE of ~99.8%.

References

1. "Stabilized porous silicon structure for highly stable silicon anode and methods of making" patent application, 31733-E US/PCT.
2. "Silicon-Based Anodes for Li-Ion Batteries," Sujong Chae et al. Encyclopedia of Sustainability Science and Technology, submitted.
3. "Localized Superconcentrated Electrolytes for Silocon Anode", patent application, 31472-E PCT
4. "Design nanostructured anode materials for Li-ion batteries", Xiaolin Li, Haiping Jia, Jiguang Zhang, presented in TMS 2020 Annual Meeting & Exhibition, San Diego, CA, February 24, 2020
5. "Hierarchical porous silicon structures with extraordinary mechanical strength as high-performance lithium-ion battery anodes", Haiping Jia, Xiaolin Li, Junhua Song, Xin Zhang, Langli Luo, Yang He, Binsong Li, Yun Cai, Shenyang Hu, Xingcheng Xiao, Chongmin Wang, Kevin M. Rosso, Ran Yi, Rajankumar Patel, Ji-Guang Zhang, Nat Commun 11, 1474 (2020). https://doi.org/10.1038/s41467-020-15217-9.

Eutectic Electrolytes for Silicon Electrodes (ANL)

John Zhang, Sisi Jiang (ANL)

Background

In this quarter we explored alternative electrolyte systems for our programmatic baseline silicon anode base don room temperature ionic liquids (RTIL). An N-methyl-N-propyl piperidinium-FSI(PMpipFSI) deep eutectic solvent (DES) material was synthesized using one-step synthesis reaction with high purity[1]. Two PMpipFSI electrolytes with 1 M and 5 M LiFSI different were prepared. The impact of the DES electrolyte on the Si interfacial stability was studied by using Si/Li half cells.

Results

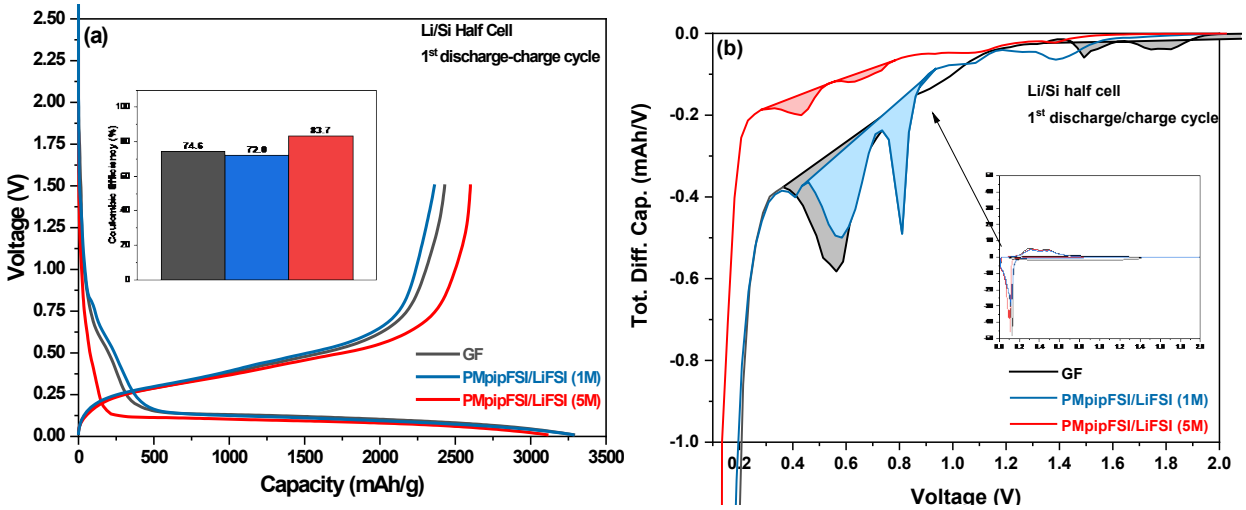

Figure 1. Electrochemical performance of Li/Si cell during initial C/20 formation cycle. (a) Voltage-capacity profiles (the inset is the Coulombic efficiencies of 3 formation cycles) and (b) differential capacity profiles.

Figure 1a are the voltage profiles of the first galvanostatic discharge-charge cycle of Li/Si half cells cycled in GF, 1 M and 5 M PMpipFSI/LiFSI electrolyte, respectively, with cutoff voltage 1.5 – 0.01 V. GF and 1 M PMpipFSI/LiFSI cells show similar features on voltage profiles with an abrupt voltage drop before 1.0 V followed by two kinks at around 0.80 V and 0.60 V and the typical flat plateau in the 0.2−0.01 V corresponding to the transition from crystalline Si to amorphous Li_xSi. In contrast, cell cycled in 5 M PMpipFSI/LiFSI experienced a polarization until 0.2 V with only slight slope change before reaching the flat plateau at around 0.15 V. The difference between high and low salt DES or GF is likely to be closely related to the difference in formation of passivation film during the initial lithiation as is indicated by differential capacity profiles in **Figure 1**b. Cell cycled in GF shows FEC reduction at 1.75 V (*vs* Li^+/Li thereinafter), EC reduction at 1.50 V and one broad reduction peak at 0.8 – 0.6 V and cells cycled in 1 M features one sharp reduction peak at 0.81 and one broad reduction peak at 0.58 V, related to anion FSI- reduction, contrasting with the cell cycled in 5 M with only negligible reduction peaks at similar voltage as 1 M. Correspondingly, 5 M cell showed the highest Coulombic efficiency (83 %), which is almost 10% higher than the other two cells, and also the highest initial reversible capacity. Apparently, passivating behavior of electrolyte on silicon anode surface depends not only on the type of electrolyte but also on the concentration of salt in the same type of solvent.

The impact on interfacial stability was also reflected on the cycles. After the three C/20 formation cycles, the cells were subjected to 100 C/10 cycles. **Figure 2** shows the voltage-capacity curves during this process, which

resembles one another originally, containing two pairs of redox peaks locating at around 0.23/0.28 V and 0.08/0.28 V, respectively, corresponding to the lithiation of Si. However, as cycles progressed, the two redox

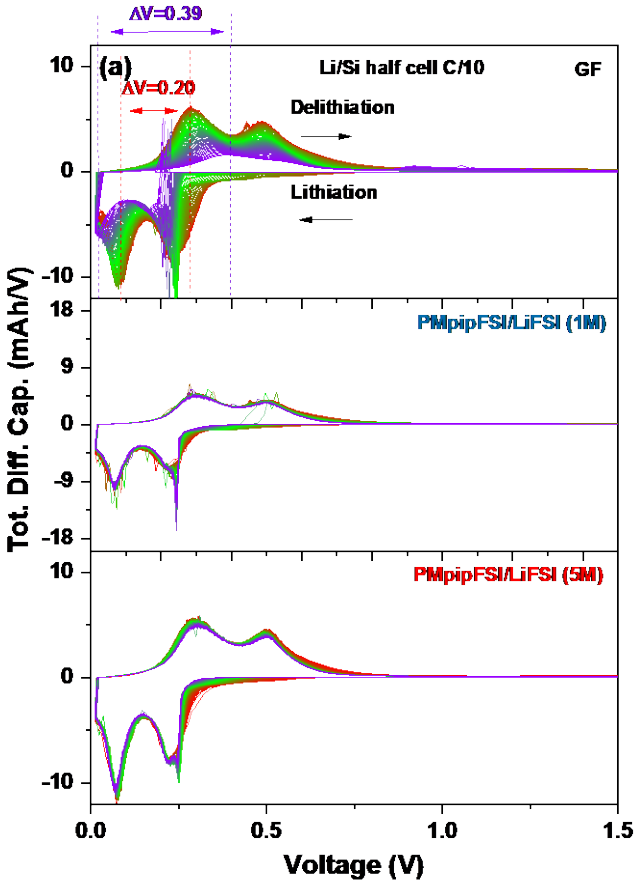

Figure 2. Electrochemical performance of Li/Si cell cycled in different electrolytes during the following 100 C/10 cycles plotted as Voltage vs capacity

peaks of GF cell gradually transitioned to 0.16/0.39 V and 0.01/0.40 V with the two oxidation peaks almost merged into one at the 100th cycle. This dramatic peak transition indicated continuous overpotential buildup as a result of side reactions during cell operation. In addition, the potential separation between the 2nd reduction and oxidation peak increases from 0.20 V to 0.39 V, which is probably caused by the change in activity of lithium ions and electrons due to the unstable interfacial condition. On the other hand, **Figure 3** shows the curves of two DES cells that remain almost unchanged from cycle 1 to cycle 100. As can be expected, the capacity retentions of DES cells by the end of 100 cycles (82% for 5 M and 81% for 1M) are much higher than that of GF cell (33%) with a higher Li+ reversibility for each cycle (average CE 99.2% for DES cell verse 96.7% for GF cell). What is worth mentioning is that although 1 M cell show comparable initial electrochemical performance as GF cell, the capacity retention is much higher than that of GF cell, indicating the difference in the stability of the passivation film formed by the two electrolytes. In addition, the impact of salt concentration of DES is not reflected on the overall performance of Li/Si cell despite the difference in surface reactivity due to the unlimited Li inventory in Li/Si cell.

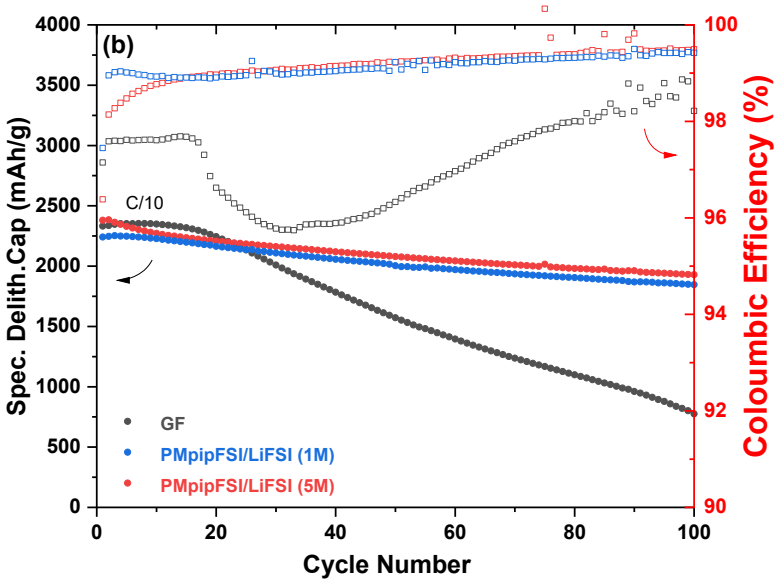

Figure 3. Electrochemical performance of Li/Si cell cycled in different electrolytes during the following 100 C/10 cycles plotted as specific delithiation capacity and the corresponding CE.

Conclusions

In sum, the interface formed between silicon anode and DES is more chemical and electrochemical stable than organic carbonate solvent. As a result, the capacity retentions of DES cells (82% for 5 M and 81% for 1 M) are much higher than that of GF cell (33%) with a higher Li^+ reversibility for each cycle (average CE 99.2% for DES cell verse 96.7% for GF cell). We will conduct EIS measurements and post-test analysis including SEM, FTIR and XPS, *etc* to further study the chemical and morphology of the SEI.

[1] Q. Liu, W. Jiang, M. J. P. Munoz, Y. Liu, Z. Yang, I. Bloom, T. L. Dzwiniel, Y. Li, K. Z. Pupek, Z. Zhang, *ACS Applied Materials & Interfaces* **2020**.

Composite Silicon-Tin Anodes for Lithium-Ion Batteries (LBNL)

Wei Tong (LBNL)

Background

We have developed reliable processes for producing amorphous Si and Si-Sn composite thin films by magnetron sputtering. Such thin films free of binder/conductive carbon additive offer the opportunity to enable the effective characterization of Si-based electrodes upon their reaction with Li. Comparatively, the Si-Sn electrode consistently exhibits better cycling performance than Si films of similar thickness during the early 20 cycles. The compositional effects for co-sputtered Si_xSn_{1-x} ($0.45 \leq x \leq 0.87$) films have been investigated in detail and the optimal Si content is determined to be x = 0.8 based on combined X-ray diffraction (XRD), scanning electron microscopy (SEM), and electrochemical testing. Here, we provide further discussions on characterizing the co-deposited Si-Sn films in terms of gravimetric capacity and long-term cycling.

Results

As previously reported, the Si_xSn_{1-x} composite thin films were directly deposited onto Cu foils by co-sputtering a Si target and a Sn target simultaneously, where the film composition was tunable by controlling the deposition power level. All the as-deposited films were subsequently stored under vacuum to prevent air exposure. 2032-type coin cells were assembled using the as-produced films (1.6 cm^2) directly as the working electrodes, Li metal foil as the counter electrode, and 1.2 M $LiPF_6$ in ethylene carbonate-ethyl methyl carbonate (3:7 by weight) as the electrolyte (Gen2). The cells were galvanostatically cycled between 1.5 and 0.01 V at C/20 based on the experimental capacity.

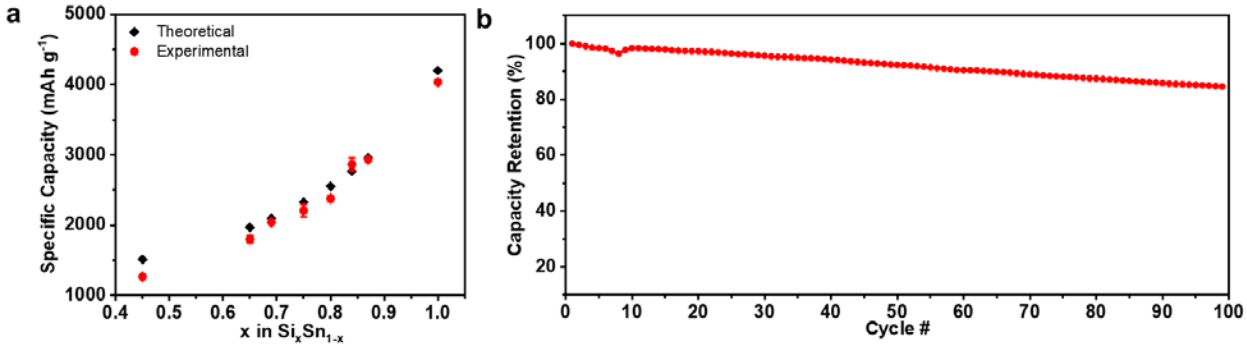

Figure 1. (a) Theoretical and experimental lithiation capacity of Si_xSn_{1-x} ($0.45 \leq x \leq 1$) films. (b) Long-term cycling performance of a Si-Sn thin film (x = 0.8).

The specific gravimetric capacity of the composite Si-Sn films as well as a pure Si film during initial lithiation is estimated based on the measured film thickness and the theoretical density of Si and Sn. The calculated theoretical capacity and experimental 1st lithiation capacity are plotted in **Figure 1a**. It can be seen that all films with $x \geq 0.69$ attain a high capacity of over 2000 mAh g^{-1}. A large difference between the theoretical and experimental values is found for the film with x = 0.45. This may be attributed to the inhomogeneous Li insertion occurring in the crystallized film, leading to incomplete reactions. The capacities of other X-ray-amorphous films are close to their theoretical capacities, regardless of composition. It can be inferred that for thin films, amorphous nature is beneficial to more complete reactions, i.e. a higher utilization of the active material.

While enhanced cyclability of Si electrodes could be achieved by limiting the cycling capacity within a narrow voltage range, we demonstrate that the Si-Sn composite film, while approaching nearly full lithiation, can cycle well in the long term at the optimal composition. As shown in **Figure 1b**, a representative coin cell containing the film with x = 0.8 is capable of retaining 84% of its reversible capacity after 100 cycles, corresponding to an

average capacity loss of around 0.16% per cycle, exhibiting excellent cycling stability on a Si-Sn composite thin film with no use of polymer binder, carbon, or FEC electrolyte additive.

Conclusions

The experimental gravimetric capacity of the co-sputtered Si_xSn_{1-x} ($0.45 \leq x \leq 0.87$) thin films is calculated and compared with their theoretical capacity. It is found that for $x \geq 0.69$, all films exhibit nearly full lithiation with a high capacity of over 2000 mAh g^{-1}, while the crystalline film of $x = 0.45$ has a lower degree of lithiation due to incomplete reactions. The optimal composition ($x = 0.8$) achieves stable cycling without use of binder, conductive carbon, or FEC electrolyte additives. Interfacial studies on the Si-Sn vs. Si electrodes in an air-free environment and exploration for novel metal additives for Si anodes based on the predictions by first-principles calculations will be pursued in the future work.

Investigating *in-situ* Ternary Li-Mg-Si Zintl Phase Formation and Evolution

Baris Key, Xiang Li, Fulya Dogan, Niya Sa (UMass), Steve Trask , James A. Gilbert, Jack Vaughey (ANL)

Background

Stable Li-M-Si ternary phases with lower chemical reactivity than simple lithium silicides helps stabilize the Si anode surface structure and reduce side reactions with electrolyte that benefits the observed electrochemistry. The ternary phase identified can be formed by adding multivalent cations (such as Mg^{2+}, Al^{3+}, Ca^{2+}, etc.) into the electrolyte in an in-situ manner. To understand the mechanism of Zintl phase formation and its dynamics, electrochemical testing, EQCM, and high-resolution ^{7}Li & ^{29}Si NMR are utilized on coin cells and pouch cell samples.

Previously we combined various types of spectroscopic and structural data to propose a mechanism of ternary phase formation in conjunction with the Han Group at NREL. From these studies we proposed that upon discharge, two slightly driving mechanisms are proposed:

(a) Exchange $Li_{3.75}Si + 0.1Mg^{2+} \Rightarrow Li_{3.55}Mg_{0.1}Si + 0.2Li^{+}$,
(b) Competition $Li_{3.55}Si + 0.1Mg^{2+} \Rightarrow Li_{3.55}Mg_{0.1}Si$

While upon charge, most data suggests that the mechanism is a simple delithiation reaction with retention of the Mg in the charged silicon anode (possibly in a metastable state):

(c) $Li_{3.55}Mg_{0.1}Si \Rightarrow Li_{3.55}\text{-}xMg_{0.1}Si + xLi$

Results

Previously we have reported that Li-M-Si (M=Mg,Al,Ca, Zn) ternary phases (Zintl phases) can be formed by co-insertion of M cations in an in-situ fashion during lithiation process, leading to less reactive and more redox stable ternary lithium silicide and enhanced long-term cycling performance.[1] However, the formation mechanism and the fundamental chemistry such as, how the dynamic changes upon charge and discharge behind this, is still unknown. Traditional diffraction techniques are especially sensitive to heavy atoms and those materials with long range order, which cannot provide true insights into the Li-related structure and the very amorphous Si phases after cycling. Nuclear Magnetic Resonance (NMR) is a powerful tool to determine the local structural environments of nuclei such as ^{7}Li, ^{31}P, and ^{19}F.[2] In this work, we comprehensively study the electrochemical lithiation of a baseline Paraclete Energy Si anode at multiple charge states to gain insights into Zintl phase formation mechanisms. In addition, the electrochemical data obtained from coin cells and pouch cells are in agreement with each other and with our former findings.

In the 1st cycle electrochemical profiles, high resolution ^{7}Li NMR spectra and the corresponding spectral simulation from unwashed pouch cells are shown in **Figure 1**. Four main Li resonances are observed and analyzed: the black peak around 0 ppm is from the residual diamagnetic Li salts in electrolyte as well as electrolyte decomposition products; the relatively sharp and narrow component at -1 ppm is assigned to Li^{+} in surface Si-O layer; Li^{+} in isolated Si is at 8 ppm; and Li^{+} in Si clusters resonates over 13 ppm. These peak assignments are consistent with our previous ex-situ ^{7}Li NMR studies on coin cells. The electrochemical profiles are very similar for both GF and GFM electrolytes when the cells are only discharged to 100 mV, while GF shows slightly higher (~30 mAh/g) specific capacity. As a result, most Li ions are inserted into isolated Si (and/or extended silicon clusters) with 97.1% in GFM and 97.8% in GF. When completely discharged to 10 mV, as seen in **Figure 3**(a), although GF and GFM share the similar discharging profile, GF cell holds more Li ions (~140mAh/g) than GF. At this stage, Li insertion into Si clusters as well as possible migration from isolated Si, and eventually forms over-lithiated Si phases. Upon charge, Li extraction preferentially take place in over-lithiated Si phases, then Si clusters and finally isolated Si, which correlates well with the coin cell data. When

charged to 400 mV, GF and GFM series represent Li removal hysteresis to different extents. There is still 24.7% Li in Si clusters and 57.7% Li in isolated Si in GFM cell, compared with almost all Li in isolated Si in GF cell. At the fully charge state, spectra shift toward lower frequency, indicating reversible Li dynamics.

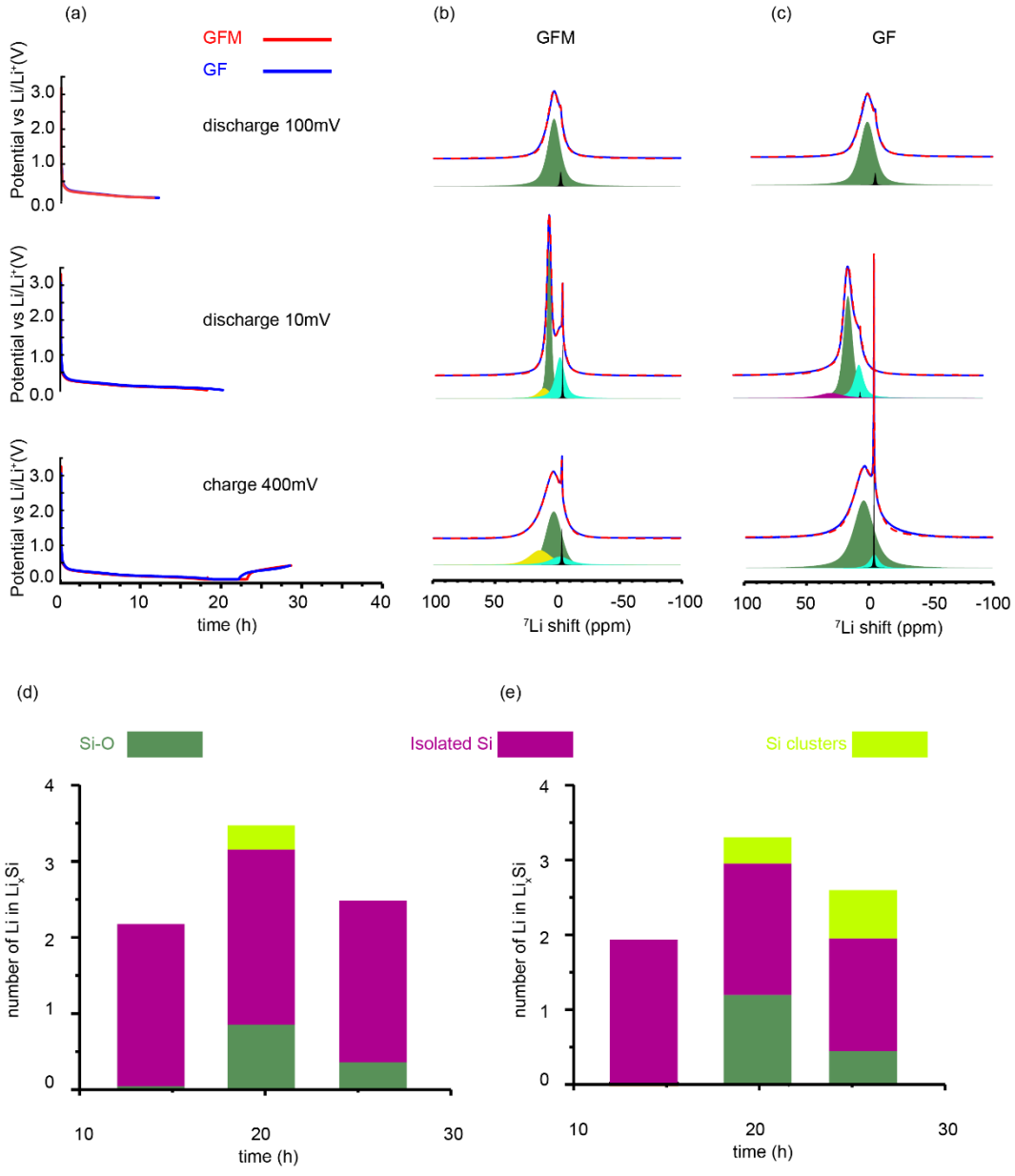

Figure 1. Electrochemical performance of GF and GFM at 100 mV, 10 mV, and 400mV (a), Experimental data (solid line) and simulation (dash line) of GFM(b) and GF(c), Li quantification with GF (d) and GFM (e) electrolytes.

^{7}Li NMR spectra comparison between pouch cells and half cells is shown in **Figure 2**. At the early state (above 100 mV), there is no significant difference except broader line shape for pouch cells which is due to the relatively lower MAS rate (20 kHz) of the NMR experiment when compared with that of coin cells.(60 kHz) However, at the fully discharge state, both GF and GFM spectra show significant differences compared to the results for the coin cells. More Li content was found to be in SEI and Si-O layer in pouch cells, which is likely due to fact that

pouch cells have significantly more amount of electrolyte and larger surface area, leading to more side reactions on the surface and SEI formation. As shown in **Figure 1** (b), **Figure 2**(b) and **Figure 3**, 52.9% Li in isolated Si and 10.8% Li in Si clusters indicate that ternary phase formation may require more Li insertion into Si clusters as well as over-lithiated Si. In contrast, with additional 140 mAh/g discharge capacity, GF pouch cell spectrum shifts to lower field and shows over-lithiated Si at 22 ppm. Longer voltage hold at 10 mV may be accelerating co-insertion of Mg^{2+} and Li-Mg-Si ternary formation in GFM cells.

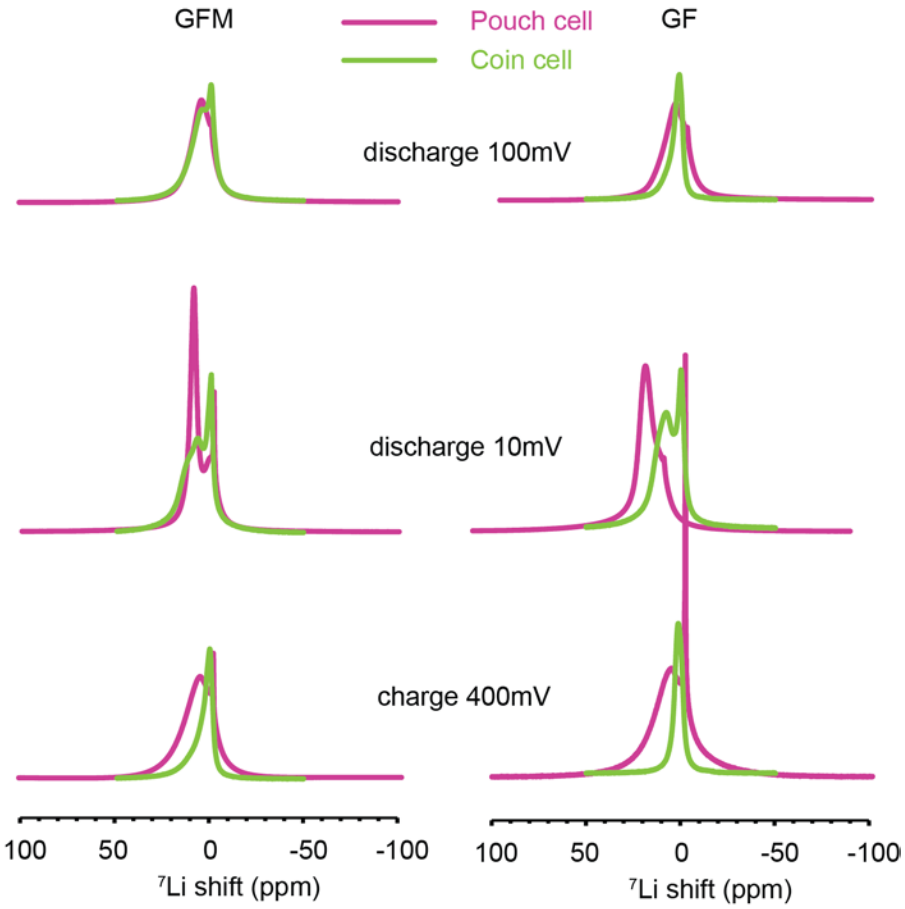

Figure 2. (a) ^{7}Li NMR spectra comparison between pouch cells(purple) and coin cells(yellow) for GFM and GF.

In **Figure 3**, the discharge electrochemistry of baseline Paraclete Si is characterized by two distinct voltage plateaus at 230 mv and 100 mV, which are corresponding to a two phase reaction: an irreversible dissociation of amorphous Si and a crystalline phase formation of $Li_{15}Si_4$. Voltage hold at 10 mV before delithiation is designed to break up all crystalline $Li_{15}Si_4$ and form amorphous Li_xSi upon charge representing a broad voltage peak at 280 mV. Note that, although GF and GFM share similar voltage profiles, subtle shift towards lower voltage at 100 mV might be a sign of Mg co-insertion. During deeper discharging process below 100 mV, Mg^{2+} could participate in lithiation to form Li-Mg-Si ternary by two possible mechanisms:

(1) $Li_{3.75}Si + 0.1Mg^{2+} \Rightarrow Li_{3.55}Mg_{0.1}Si + 0.2Li^{+}$

Li ions continue coordinating with Si and form crystalline $Li_{3.75}Si$ first, ion exchange between Li^{+} and Mg^{2+} is driven by low potential.

(2) $Li_{3.55}Si + 0.1Mg^{+2} \Rightarrow Li_{3.5}Mg_{0.1}Si$, which is more likely from electrochemical perspective due to slighly lower overall lithiation capacities observed during the discharge for GFM.

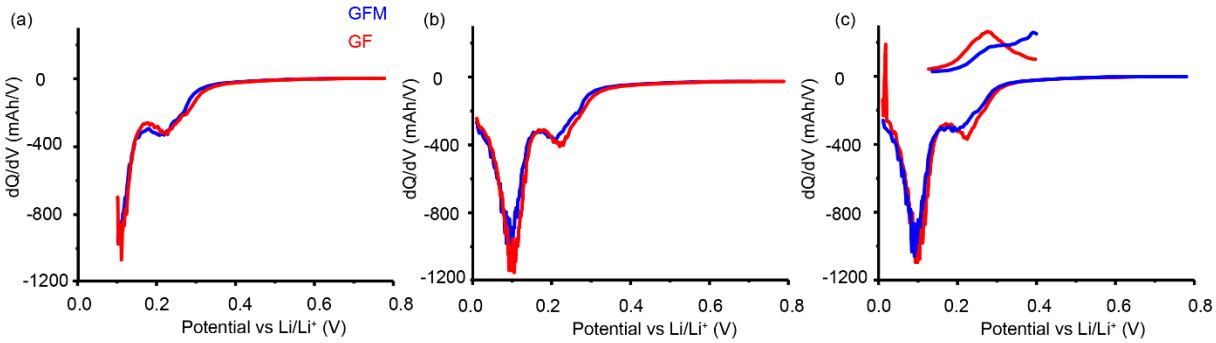

Figure 3. Differential capacity vs voltage plots of GF and GFM at 100 mV (a), 10 mV (b) upon discharge, and 400 mV (c) upon charge.

To further understand the mechanism of the Zintl phase formation, an *in-situ* Electrochemical Quartz Crystal Microbalance measurement with Dissipation mode (EQCM-D) is applied to a Si thin film anode free of binder and conductive carbon vs Li metal in two electrolyte environments, GenF and GenFM. **Figure 4** presents simultaneous electrochemical lithiation voltage from OCV=2.5 V to 0.015 V with the corresponding frequency difference at the 3rd overtone. Two lithiation stages are monitored, the pre-lithiation process for SEI formation from 2.5 V to 350 mV and the post-lithiation stage from 350 mV to 15 mV. Results suggest before lithiation occurred (>350 mV), the frequency shift for the GenFM electrolyte is less significant than for the GenF electrolyte suggesting the SEI formation is less protuberant with the Mg addition in comparison with the GenF electrolyte. Frequency shift is mainly contributed from the electrolyte reduction as well as lithium insertion into surface SiO in agreement with the ssNMR finding. For the post-lithiation stage (100 mV to 15 mV), frequency shift for the GenFM electrolyte at lowered voltage range from 100 mV to 50 mV is more significant than the GenF electrolyte and this trend is opposite in contrast to the pre-lithiation stage. Lithiation of Si into $Li_{3.75}Si$ gives a mass increase of 48% of the reaction, however, formation of the ternary Zintl phase and the magnesiation of $Li_{3.75}Si$ to form $Li_{3.55}Mg_{0.1}Si$ phase merely gives a mass increase of 1.9%. Consequently, the apparently decreased frequency shift with the Mg addition occurring at lowered voltage range from 100 mV to 50 mV clearly suggests that a partial inclusion of Mg and formation of the Li-Mg-Si ternary occurring in parallel in addition to the lithiation of Si.

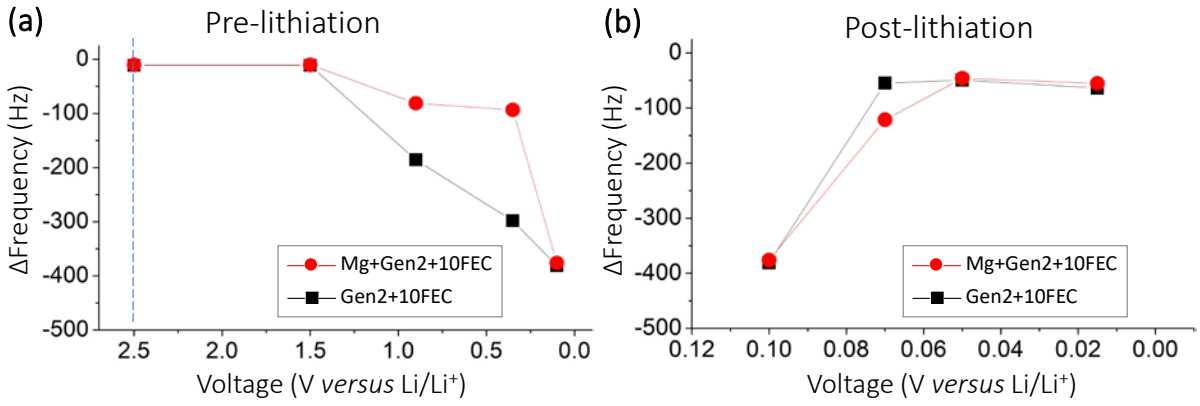

Figure 4. Correlation of the lithiation voltage versus the frequency difference from in-situ EQCM measurement of a 50 nm Si thin film vs lithium metal in GenF (black square) and GenFM (red circle) electrolyte. (a) pre-lithiation stage at V>350 mV; (b) post-lithiation stage at V < 350 mV.

Finally, limited preliminary calendar life hold tests were performed on 80% Si CAMP electrodes in full coin cells (vs. NMC532) with the procedure in **Figure 5**. Comparison of parasitic currents for GF and GFM suggests

significantly better passivation for system with magnesium consistent with EQCM results. Immediate follow-up studies will focus on more stable cycling electrodes and long calendar life tests utilizing various multivalents with long cycle life targets.

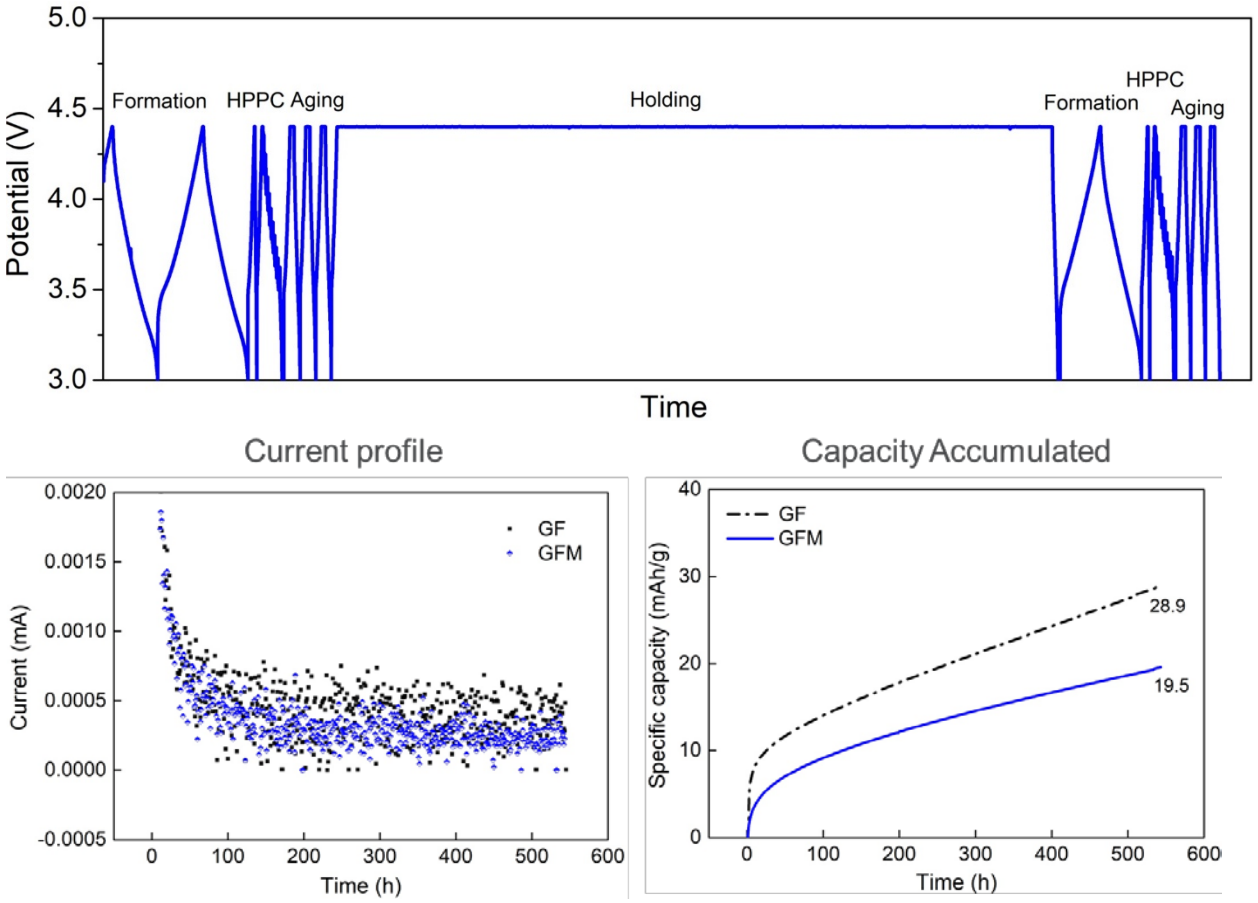

Figure 5. Preliminary calendar life test protocol and current and capacity plots during the 540 hour voltage hold step for GFM and GF electrolytes

Conclusions

The evolution of Li and Si local environments for pure Si anode in two different electrolytes were investigated using EQCM, *ex-situ* ^{7}Li and ^{29}Si MAS NMR. Li-Mg-Si ternary phase formation requires large amounts of Li insertion into Si clusters, it could be accumulated by holding the voltage at sufficiently low voltage, such as 10 mV. A more even Li distribution and lower electrochemical hysteresis were promoted by Li-Mg-Si ternary phase formation at the interface. Electrochemistry performance from scale-up pouch cells are consistent with lab-scale coin cells. We propose that upon discharge Li-Mg-Si ternaries form uniformly preferably by competition between Li and Mg only at deeply lithiated stages; upon charge, Mg remains in the bulk forming Li poor or completely lithium deficient $Li_xMg_{0.1}Si$ phases and contribute to stable ternary phases in subsequent cycles. The promising potential for scale-up applications examined by pouch cell testing, as well as offers more stable passivation at high states of charge in full cells which should yield to longer calendar life for optimized electrodes which will be the immediate focus in the next quarter.

References

1. Key, B. *et al.* Real-Time NMR Investigations of Structural Changes in Silicon Electrodes for Lithium-Ion Batteries. *J. Am. Chem. Soc.* **131**, 9239–9249 (2009)

2. Pecher, O., Carretero-González, J., Griffith, K. J. & Grey, C. P. Materials' Methods: NMR in Battery Research. *Chem. Mater.* **29**, 213–242 (2017).

Mechanistic Studies of Zintl Electrolyte Additives on SEI (UMass/ANL)

Niya Sa (UMB), Saida Cora (UMB), J. Vaughey (ANL)

Background

Our major focus this quarter was to provide an in-depth analysis of the early SEI formation mechanism with multivalent Mg ion addition to a Si thin film anode. The work was performed in collaboration with the MAS-NMR team at Argonne led by Baris Key, where we used a variety of spectroscopic tools to identify mechanistic aspects of surface Zintl formation on silicon anodes. Work performed in this quarter is divided into three parts, with the goal to (1) quantify the initial SEI formation mechanism; (2) understand the dynamic role of the Mg^{+2} additives to the early SEI formation; (3) evaluate the concentration effect from the Mg addition to the coulombic efficiency of the Si thin film anode.

Results

Major focus in this quarter is to distinguish the pre-SEI formation ascribed from electrolyte reduction and the post-SEI formation after lithiation and de-lithiation, in various electrolytes for model Si anode with EQCM-D. An in-depth data analysis for the electrolyte dependent SEI formation as well as its voltage dependence is performed to understand the SEI formation mechanisms.

Experimental Results and Discussion:

Theoretical mass difference for lithiation of Si in electrolyte with and without Mg addition

NMR results suggest following three reaction pathways for possible lithiation or Li-Mg-Si formation. Theoretical mass difference is firstly calculated to give an estimation change of mass for the following reaction pathways. Results suggest a mass gain of ~48% if pure lithiation is occurring, and a significantly reduced mass gain of less than 5% for Zintl phase formation of Li-Mg-Si.

Reaction 1:

$3.75Li + Si = Li_{3.75}Si$

(Si=28.0855; Li (6.941)*3.75=26.029; $Li_{3.75}Si$ = 54.114g/mol)

(If the solid phase of $Li_{3.75}Si$ is formed, a mass increase of 26.029/54.114 = 48.1%gain)

Li=6.941; Si=28.0855; Mg=24.305

Reaction 2:

$Li_{3.75}Si + 0.1Mg^{2+} = Li_{3.55}Mg_{0.1}Si + 0.2Li^{+}$

($Li_{3.75}Si$ = 54.114, 0.1Mg = 2.43; $Li_{3.55}Mg_{0.1}Si$ = 24.641+2.43+28.0855=55.1565, mass gain%=1.9%)

Reaction 3:

$Li_{3.5}Si + 0.1Mg^{+2} \rightarrow Li_{3.5}Mg_{0.1}Si$

(if $Li_{3.5}Mg_{0.1}Si$ is formed: 6.941*3.5+28.0855=52.379, $Li_{3.5}Mg_{0.1}Si$=54.809; mass gain%=4.5%)

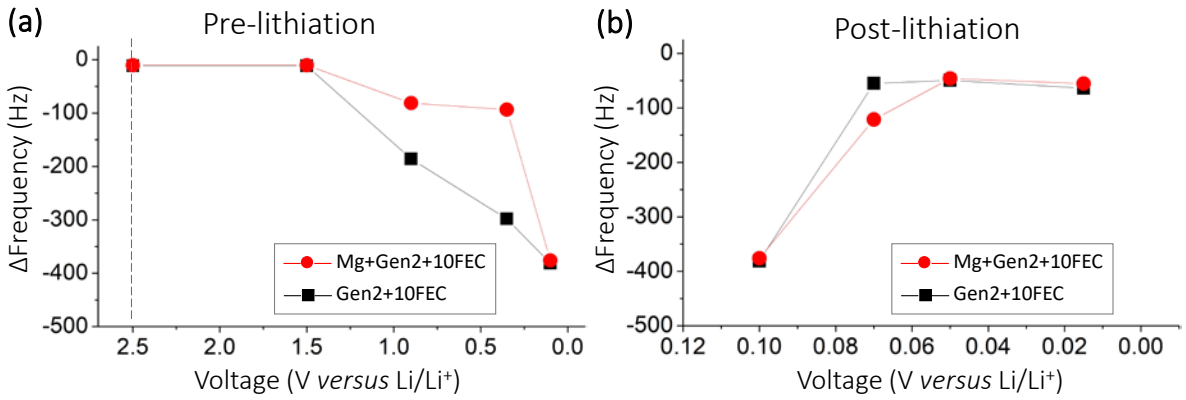

Figure 1. Correlation of the lithiation voltage versus the frequency difference from the *in-situ* EQCM measurement of a 50 nm Si thin film vs lithium metal in GenF (black square) and GenFM (red circle) electrolyte. **(a)** pre-lithiation stage at V>350 mV; **(b)** post-lithiation stage at V < 350 mV.

EQCM-D Analysis of the *in-situ* Zintl Phase Formation

To further understand the mechanism of the Zintl phase formation, an *in-situ* Electrochemical Quartz Crystal Microbalance Measurement with Dissipation mode (EQCM-D) is applied for a Si thin film anode free of binder and conductive carbon vs Li metal in two electrolyte environments, GenF and GenFM. **Figure 1** presents simultaneous electrochemical lithiation voltage from OCV=2.5 V to 0.015 V with the corresponding frequency difference at the 3rd overtone. Two lithiation stages are monitored, the pre-lithiation process for SEI formation from 2.5 V to 350 mV and the post-lithiation stage from 350 mV to 15 mV. Results suggest before lithiation occurred (>350 mV), the frequency shift for the GenFM electrolyte is less significant than for the GenF electrolyte suggesting the SEI formation is less protuberant with the Mg addition in comparison with the GenF electrolyte. Frequency shift is mainly contributed from the electrolyte reduction as well as lithium insertion into surface SiO in agreement with the ssNMR finding. For the post-lithiation stage (100 mV to 15 mV), frequency shift for the GenFM electrolyte at lowered voltage range from 100 mV to 50 mV is more significant than the GenF electrolyte and this trend is opposite in contrast to the pre-lithiation stage. Lithiation of Si into $Li_{3.75}Si$ gives a mass increase of 48% of the reaction, however, formation of the Zintl phase and the magnesiation of $Li_{3.75}Si$ into $Li_{3.55}Mg_{0.1}Si$ phase merely gives a mass increase of 1.9%. Consequently, the apparently decreased frequency shift with the Mg addition occurring at lowered voltage range from 100 mV to 50 mV clearly suggests that a partial inclusion of Mg and formation of the Li-Mg-Si ternary occurring in parallel in addition to the lithiation of Si.

Conclusions

In this quarter we evaluated the role of magnesium concentration on the initial stages of SEI formation. Specifically over a range from 0-200 mM Mg^{+2} addition to standard Gen2 electrolyte, significant differences were seen. Notably the SEI forms earlier in higher concentration Mg salts, and is generally much thinner with Mg^{+2} inclusion.

Soluble SEI Species

Chen Fang, Gao Liu (LBNL)

Background

Silicon anode has promising applications for lithium ion batteries (LIBs) due to its high theoretical specific capacity of 3590 mA h g−1 based on the fully lithiated form of stoichiometry $Li_{15}Si_4$, which is over a magnitude higher than of conventional graphite anode. However, the full utilization of Silicon's capacity has not been realized due to the lack of understanding of solid electrolyte interphase (SEI) formation, which is closely associated with electrolyte decomposition and is crucial for stabilization of the silicon negative electrodes. In the past, a broad range of organic electrolyte molecules as well as organic additive molecules have been explored for silicon-based LIBs but their precise electrochemical decomposition products had rarely been determined. The objective of the present study is to develop facile analytical protocols for unambiguous identification of organic species such as polymers in SEI layers.

Previously, we have established the gradient polarity solvent wash (gradient wash) technique. This is an on-electrode chromatography strategy that can realize sequential removal of different SEI and near SEI components in different fractions based on their molecular properties. Here, we combine the on-electrode chromatography technique with MALDI mass spectrometry, the latter of which can provide additional information about the polymers such as molecular weight and repeating unit.

Results

In the present study, we examine the impact of the common anode passivation compound vinylene carbonate (VC) on decomposition of electrolyte molecules that leads to polymer formation. The scheme is shown in **Figure 1**. The initial results based on VC additives carried out on-electrode chromatography by gradient wash of Cu electrodes cycled in Gen2 electrolyte ($LiPF_6$ in EC/EMC) with or without VC was reported in FY20 Q2. According to FTIR measurements reported, after treatment with 3:7 ethyl acetate (EA):hexane (Hex) solution,

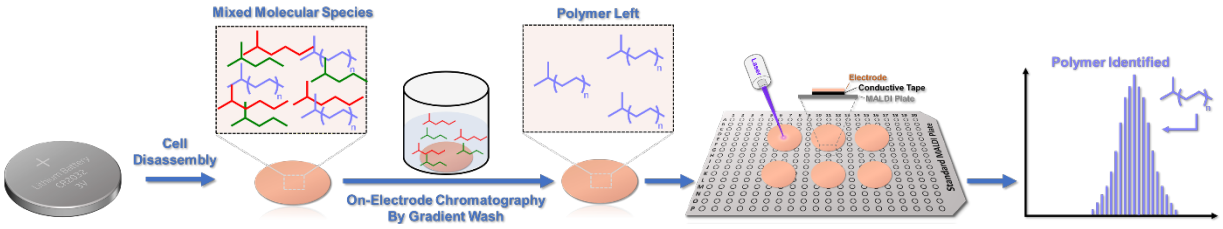

Figure 2. Scheme of methodology used in the project

the electrode cycled with Gen2 had the residue electrolyte removed while the electrode cycled with Gen2/VC appeared to have polyethylene oxide (PEO). This result was further confirmed with MALDI measurements. The electrode cycled with Gen2 shows extremely weak signal of PEO while the electrode cycled with Gen2/VC shows very strong PEO repeating patterns. The mass matches the linear PEO species that have been proposed in literature with one or two terminal carbonate groups.

This technique had been applied to the SEI of silicon cells using the baseline electrolytes in the DeepDive program. However recent work by Key, Sa, and Vaughey has highlighted that the SEI formed in the presence of Mg electrolyte salts is thinner and more compact than that naturally formed. Key has also noted that the surface appears more stable due to ternary Zintl phase formation (a ternary phase in the Li-Mg-Si system) and that the corrosion current associated with silicon electrodes is diminished by an order of magnitude (see **Figure 2**). Mechanistic studies by Sa and Key have highlighted the mechanism of formation of these phases but to this point how they change the interaction with the electrolyte is only proposed. In a collaborative effort with Argonne and UMass, we are in the process of examining the materials formed during SEI formation in these systems to determine the differences in species formed and the role of the new in-situ surface coating on the

significant decline in corrosion currents. Results on identifying the phase distribution formed and the differences to standard electrolytes will be noted and will be reported in future quarters.

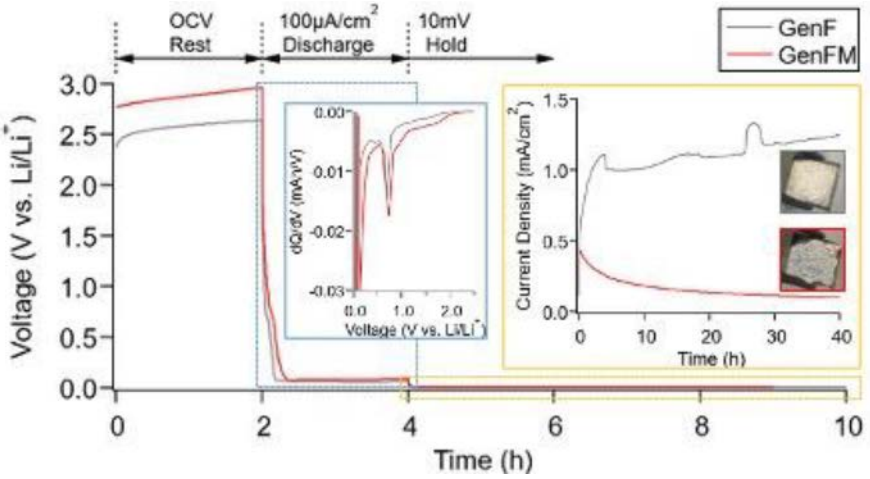

Figure 2. Demonstration that addition of Mg salts to Gen2F diminishes the parasitic currents seen for typical silicon cells.

Conclusions

In summary, the combination of on-electrode chromatography by gradient wash and MALDI proves to be a convenient and powerful technique for identification of polymer species as electrolyte decomposition products on the electrode surface. The next step is to investigate FEC, the most used Si additive, decomposition patterns during the electrochemical processes and the SEI formed when the Zintl phase ifs formed at the surface of the anode in collaboration with Niya Sa (UMass) and Baris Key (ANL).